RESEARCH ARTICLE-CIVIL ENGINEERING

Fly Ash and BOF Slag as Sustainable Precursors for Engineered Geopolymer Composite (EGC) mixes: A Strength Optimization Study

Saravanan Subramanian[1] · Tirumalasetty Dhathu Eswar[1] · Vinay A Joseph[1] · Sneha B Mathew[1] · Robin Davis[1]

Abstract

Engineered geopolymer composites (EGC) have emerged as a more environmentally friendly alternative to conventional engineered cementitious composites (ECC). These composites offer high mechanical and durability features. However, there is a lack of research on EGC, particularly with basic oxygen furnace (BOF) slag as a precursor and iron ore tailings (IOT) as a partial replacement to fine aggregate. Despite their effectiveness as industrial waste products in conventional concrete, this study aimed to determine the optimal compositions of fly ash (FA), steel fibres (SF), and IOT by varying their percentages. Overall, 150 mix combinations were tested, including six binder combinations, five combinations of fine aggregates, and five percentage variations in SF. Finally, one optimum mix was selected for each binder combination, based on the ultimate compressive strength values corresponding to the six optimal mixes. The compressive strengths of all the mixes were evaluated at both 7 and 28 days of curing, involving three replicate samples after oven curing (initial 24 h) followed by subsequent ambient curing until their respective ages. The highest observed compressive strength after 28 days was 41.77 MPa for 50 mm cubes. This strength was achieved with a composition of 60% FA, 1.5% SF, and 45% IOT. An increase in IOT percentage led to a nearly linear increase in strength, while the strength peaked at 1.5% for steel fibres. The addition of BOF slag significantly enhanced the compressive strength compared to mixes with full FA. A 40% fly ash replacement with BOF slag resulted in an average strength that was 39% higher than the combination with 100% fly ash. However, the strength growth decreased after a 10% replacement. Analysis of variance was conducted using the design of experiments methodology to determine the significance of the parameters and their interactions. All three independent parameters were found to be statistically significant, while their interactions were not. Utilizing Taguchi's analysis method with the L25 orthogonal array, it was concluded that IOT percentage was the most influential parameter.

Keywords Engineered geopolymer composite (EGC) · Basic oxygen furnace (BOF) slag · Steel fibres (SF) · Fly ash (FA) · Iron ore tailings (IOT) · Optimization · Taguchi's method · ANOVA

1 Introduction

Cement concrete has long been a predominant material in the construction industry, finding extensive application across various domains. However, despite its versatility and widespread usage, the environmental and ecological impacts associated with its production are substantial. The primary concern revolves around the excessive consumption of cement, which leads to the emission of greenhouse gases, including CO_2, resulting in environmental degradation. The pressing need to address global warming has prompted industrialists worldwide to develop eco-friendly construction materials to help conserve rapidly depleting non-renewable resources. Research indicates that carbonate burns in cement industries contribute significantly to global greenhouse gas emissions, accounting for approximately five to eight per cent annually [1–3]. Remarkably, cement production has become the second-largest consumable after water. Statistical data further highlight that the annual production of ordinary Portland cement (OPC) increased by a staggering 2.6 billion metric tonnes [4, 5]. More notably, the emission of carbonate burns corresponds directly to the quantity of raw materials produced for each tonne of cement. In light of these facts, there is a growing urgency to address the carbon footprint associated with cement production. Efforts are underway

✉ Saravanan Subramanian
  ssarav2009@gmail.com

[1] Civil Engineering Department, National Institute of Technology Calicut, Calicut, Kerala, India

to develop sustainable alternatives and mitigate the adverse environmental impact caused by the industry's practices.

At the same time, the by-product materials like fly ash (FA), ground granulated blast furnace slag (GGBFS), basic oxygen furnace slag (BOF), iron ore tailings (IOT), from thermal and steel plants have rapidly increased and are not being effectively utilized. Global steel production has rapidly increased over the past 60 years, accounting to (~ 1666.2 million tons) relative to a mere 500 million tonnages in 1967, experiencing a significant increase of more than 200% as per the survey conducted by the World Steel Association [6]. The substantial development of steel industries globally has resulted in excess consumption of non-renewable sources, resulting in environmental degradation by their residues and improper utilization and disposal of the same [7, 8]. Steel industries have been utilizing almost 5–6% of global energy resources [9], making them one of the main contributors to atmospheric CO_2 emissions (up to 5%) following cement production. The International Energy Agency (IEA) (2021) published a report on the iron and steel technology roadmap, which stated that the iron and steel industries account for 2.6 giga tones of CO_2 emissions annually, 7% of the global total from their production. Also, the steel sector has become the most significant consumer of coal, which provides around 75% of its energy demand [10–13].

Residual waste generation in the form of slag has been yet another primary concern in steel industries, accounting for almost 1600 million tonnage of residual waste generation majorly in the form of slag [14, 15], which is again classified based on their making process as basic oxygen furnace slag (BOF slag), electrical arc furnace slag (EAF slag), and ladle refining slag (LFS) [16], and the former one is of our interest in the production of EGC as the major precursor material following fly ash (FA). This by-product resulting from coal manufacturing has also been the material of concern regarding their availability in abundance and despite not being utilized effectively (only up to 63.28%) relative to its availability of 169 million tonnes as per an annual study for the year 2016–17 in India [17]; anyways as opposed to BOF slag, fly ash has resolved the issue on disposal management to a certain extent upon being utilized in concrete and geopolymer binders over the decades. The issues on BOF slag are adverse as their accumulation in landfills causes detrimental effects to the environment, forming a highly alkaline source marking the deterioration of water bodies and surrounding soil [18–20]. Excess utilization of non-renewable natural resources to serve the accrescent urban development has led to significant environmental damage. Nonetheless, sand being the most widely adopted material as fine aggregate, various legislations and restrictions in procuring it have made them the least opted one [21].

The requirement for an effective alternative to cater to the needs of the construction sector has become inevitable. Iron mining, one of the vital processes for developing a nation's economy, has ill effects relating to its residues (iron ore tailings—IOT) as a part of its production process. It has been statistically proven that in India, 10–12 million tonnage of IOT [22] is one of the most abundantly available solid wastes contaminating the water bodies and the surrounding ecosystem during storage and dumping [23, 24]. For these concerns, enhancing the environmental efficiency aspects alongside the reuse/recycling of residues has been the need of the hour, focusing on materials of our concern (IOT and BOF slag). Assessing the current scenario, polymer-based concrete has become the most opted viable choice to look after as an alternative to conventional ordinary Portland cement concrete (OPC), considering its superior qualities of strength, durability against adverse environments, load absorption, improved wear and tear, high early strength and their eco-efficiency characteristics by involving industrial residues. Nonetheless, this made researchers perform ample studies on geopolymer concrete (GPC) as an immediate and sustainable alternative to OPC [25–28]. However, lightweight composites viz., engineered geopolymer composites (EGC), also termed strain-hardening geopolymer composites, have been the significant material under research in recent times by deriving knowledge from its predecessors GPC and strain-hardening composites comprising cementitious derivatives or as commonly known engineered cementitious composites (ECC), characterized by enhanced engineering properties like multiple cracking behaviour and large tensile strain capacity [29–37]. Nevertheless, the latter comprises a significant quantity of ordinary Portland cement (OPC), thereby leading to excess carbon footprint. The combined knowledge gained from GPC and ECC has facilitated the development of EGC [38–44]. Multiple studies have shown that EGC, which possesses strong tensile strength and high strain capacity [38, 39, 44, 45], has the potential to be a sustainable alternative to ECC while maintaining its superior mechanical [46–48] and durability properties [49–51]. However, EGC exhibits significant variability in its precursor materials and mix proportions alone [52–55], making standardization for practical applications difficult. Previous research has primarily focused on EGC's mechanical properties by varying the precursor materials and involving commonly available by-products from thermal and steel plants [38, 39, 52, 55–63]. Also, studies on the sustainability of sand replacement are mere and, if so, involve artificial derivatives, making the resulting mix economically unfeasible. It is to be noted that no profound study has been conducted on EGC involving FA: BOF slag as its precursor, while IOT being partially replaced to the conventional fine aggregate (M-sand—in this case) and their influence on the compressive strength development by assessing their feasibility level [64].

The present study investigated the compressive strength variation of a hybrid binary blend EGC made of FA and

BOF slag as primary precursor materials and fine aggregate (M-sand) being replaced partially by iron ore tailings and involving steel fibres. The percentage replacement of BOF slag, IOT, and steel fibres over the various proposed EGC mixes has been chosen as the key parameters, thereby performing optimization studies. Fly ash was chosen as the primary precursor, and the effect of BOF slag replacement was studied. The percentage replacement of fly ash in this study by BOF slag varies from 0 to 50% (6 levels), whereas in the case of fine aggregates, IOT replaces M-sand from 0 to 45% (5 levels). The steel fibre addition varied from 0.8 to 2% (5 levels). Compressive strength test was conducted on the proposed 150 mixes. The significance of each parameter was analysed experimentally and validated by optimization techniques involving the design of experiments and Taguchi's methodology. The influential parameter on compressive strength development has been investigated. Six mixes were chosen as the final optimized mixes by selecting the ones with the highest compressive strengths for each BOF slag replacement.

2 Research Significance

Concrete has been the most commonly utilized traditional construction element involving ordinary Portland cement (OPC) binders. In recent years, engineered cementitious composites (ECC), when substituted for concrete, and geopolymer, when substituted for OPC, thereby forming geopolymer composites, have the potential to lower the significant carbon footprint of the former. However, limited past research studies have reported a variety of inferences. This paper addresses a knowledge gap by developing an engineered geopolymer composite (EGC) mix involving untouched precursors, viz., Basic Oxygen Furnace (BOF) slag and Iron Ore Tailings (IOT) as a partial replacement to fine aggregate. This study presents the optimization results of the proposed EGC based on their compressive strength assessment, involving traditional and theoretical methodologies involving Taguchi's theory and design of experiments.

3 Engineered Geopolymer Composites (EGC): Evolution

Concrete has been the most essential construction element over time; nonetheless, it has not been immune to well-documented flaws. Concrete, being brittle, possesses low tensile strength. To address this issue, the addition of fibres to concrete (fibre-reinforced concrete—FRC) is a well-established approach for reducing brittleness by minimizing fracture formation and propagation. While the addition of fibres to concrete (fibre-reinforced concrete—FRC) has been effective in enhancing tensile strength, the improvement in ductility has been relatively limited compared to engineered cementitious composites (ECC) and engineered geopolymer composites (EGC). Some FRCs may exhibit comparable tensile strengths to ECCs/EGC, but their tensile ductility can be significantly lower. Furthermore, FRC continues to exhibit a strain-softening tendency after first cracking under tensile stress, as shown in Fig. 1 [65]. As a result, high-performance fibre-reinforced cementitious composites (HPFRCC) were created as a superior option to alleviate concrete brittleness and poor tensile behaviour. Unlike FRC, HPRFRCC exhibits strain-hardening after first cracking under tensile loads. Strain-hardening usually occurs as a result of inelastic deformation of the composite by the initiation of multiple micro-cracks.

To distinguish this mechanism from the strain-hardening phenomenon usually reported in metals, this inelastic deformation occurs with an increase in load-carrying capacity, referred to as Pseudo strain-hardening (PSH). HPFRCC variants were built with high fibre contents (up to 20% by volume) and obtained desirable improvements in tensile strength and ductility. However, its substantial fibre content restricted its field deployment due to economic issues. Engineered cementitious composites (ECC) were then a novel type of fibre-reinforced cementitious composites created and optimized using micromechanical principles and as a result were proven to display improved tensile ductility of 2–5% tensile strain capacity relative to both conventional concrete and fibre-reinforced concrete involving reduced fibre content of up to 2% [66–70]. As these composites do not involve coarse aggregate in their matrix, the amount of binder (cement) consumption is high compared to conventional concrete, thereby leading to environmental deterioration as cement is the major contributor to up to 8% of global anthropogenic emissions [70]. Ongoing studies have been determinant in developing new binder materials to be incorporated in the production of ECC and thereby attaining a novel composite with strength properties analogous to the former. An efficient and sustainable replacement to cement-based binders has been proposed recently, involving geopolymer binders and the resulting composite as engineered geopolymer composites (EGC) or strain-hardening geopolymer composite (SHGC). EGC is designed and bound to display robust PSH behaviour at low fibre content, usually (< 2%) [38, 52, 55, 71, 72], using similar principles as engineered cementitious composites (ECC). According to preliminary research, EGC, like ECC, has significant tensile ductility and increased tensile and flexural strength relative to conventional fibre-reinforced concrete. However, due to the low fracture toughness of geopolymer matrices, EGC could attain improved tensile ductility at a considerably lower fibre percentage than ECC [38, 52, 55, 73, 74]. As a result, potential cost savings and greater feasibility on serviceability can be attained.

Fig. 1 Stress–strain graphs [65]
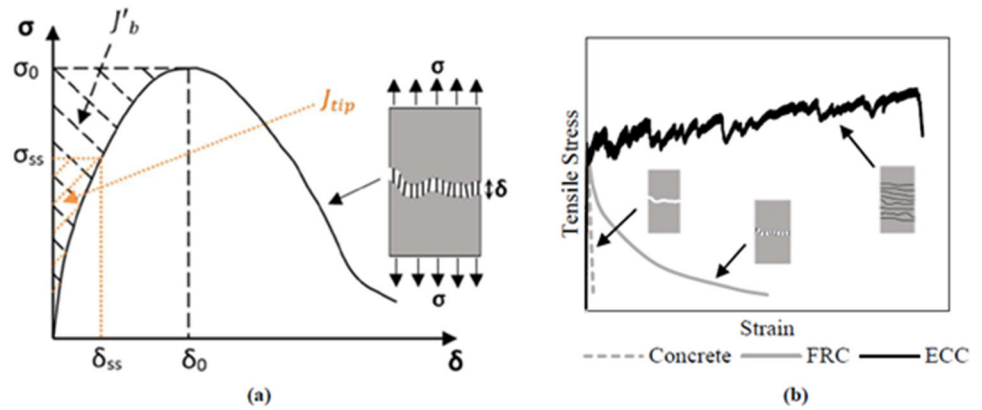
Fig. 2 Raw materials **a** steel fibres **b** BOF slag **c** iron ore tailings **d** fly ash

4 Experimental Investigation

A total of 900 cubes were cast from 150 mixes by varying the three parameters: IOT, SF, and FA percentages. The materials used, mixture proportions, and experimental procedure are explained in the following sections. 50 mm cubes were made for compressive strength testing following IS-4031-P-6:1988.

4.1 Materials and Methods

The raw materials used for this study are BOF slag (Fig. 2b) and FA (Fig. 2d) as aluminosilicate precursors, IOT (Fig. 2c) and M-Sand as fine aggregates, SF (Fig. 2a) as ductile reinforcements, and, NaOH and Na_2SiO_3 as alkaline activators. The particle size distributions of all raw materials tested at Central Instrumentation Laboratory (CIL), VISTAS, are shown in Fig. 3. This graph plots the passing percentage of these materials with the sieve size. XRF test results for BOF slag, IOT, and fly ash are shown in Table 1. Class-F, low-calcium fly ash (FA) has been utilized in this study (Fig. 2d). It was sourced from Neyveli Lignite Corporation (NLC). It has 5–10% lime conforming to standard specifications as per IS 3812 (Part 1 and 2): 2003. Basic oxygen furnace slag was used as an aluminosilicate precursor in this study. The loose and compacted bulk densities of 0.93 kg/l and 1.00 kg/l were observed when tested per IS:2386 (Part 3)-1963. The
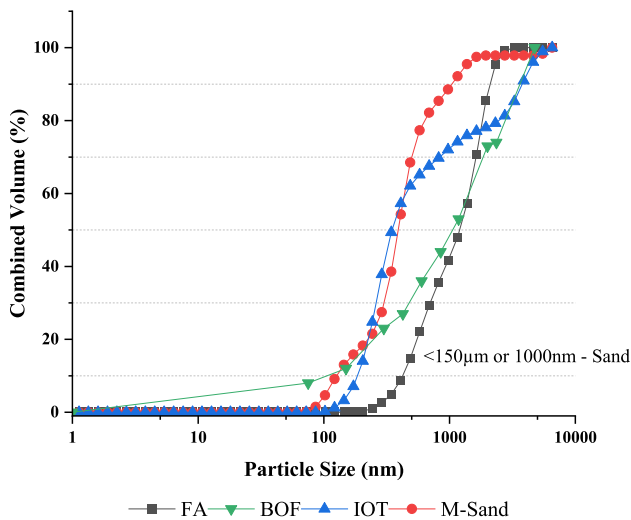
Fig. 3 Combined particle size distribution of test materials

distinctive chemical composition of BOF slag can significantly influence the mechanical properties of composites. Previous studies have shown that incorporating BOF slag in composite mixes can enhance compressive strength, improve durability, and reduce the permeability of the resulting composites [75, 76]. The higher content of SiO_2 and Al_2O_3 in BOF slag contributes to the formation of additional calcium silicate hydrate (C–S–H) gel, which enhances the overall strength and durability of the geopolymer composite. Moreover, the presence of MgO in BOF slag can contribute to the formation of magnesium silicate hydrate (M–S–H) gel, further enhancing the mechanical properties of the composites. These unique characteristics differentiate BOF slag-based composites from other slag-based composites and make it a promising sustainable alternative for construction applications.

According to IS:2386 (Part 3)-1963, aggregate testing methods were performed on IOT to measure its bulk density. A loose bulk density of 1.89 kg/l and compacted bulk density of 1.99 kg/l were observed. A specific gravity of 3.47 was observed when tested according to IS:2720 (Part 3/Sec.1)-1980. Considering the recent scenario of scarcity of river

Table 2 Properties of M-sand

Description	Manufactured sand	Standard limits as per Zone-II as per IS:383–2016
Specific gravity	2.7(SSD)	2.1 to 3.2
	2.65(OD)	
Water absorption (%)	1.9	Not more than 5%
Surface moisture	Nil	NA
Bulk density (kg/m^3)	1660	Limit not specified
Bulk density—loose condition (kg/l)	1.66	Limit not specified
Bulk density—compacted condition (kg/l)	1.75	Limit not specified

sand and the results of former studies showing the improved performance of GPC when M-sand is used [77], the same is used as a fine aggregate in this study. The various test results showing the properties of M-sand is tabulated in Table 2. These were done in accordance with IS:2386 (Part 3)-1963. The fibres used in this study were 13-mm-long brass-coated steel fibres (referred to SF, hereafter).

The mechanical properties of SF used, is shown in Table 3. The key roles of SF in the EGC is to increase the ultimate tensile load and to induce ductility. Sodium silicate, sodium hydroxide, potassium hydroxide, or a combination of the three can be used to produce geopolymer concrete mortar. However, most studies have shown that using sodium hydroxide and sodium silicate together can increase the strength of geopolymer concrete [78, 79]. The concentration of the alkali solution is also found to influence the final product's strength [80] significantly. 12 M NaOH solution was used for the study. This was made by dissolving 0.48 kg of NaOH pellets in 1 L of water. The composition of the NaOH solution is shown in Table 4. Anhydrous sodium metasilicate was used in the powdered form, which was added directly to the mixture. NaOH to Na_2SiO_3 molarity ratio of 2.5 was chosen for this experiment. The properties of sodium metasilicate are shown in Table 5.

Table 1 Chemical compositions of test materials—XRF analysis

Materials	Percentage composition (%)												
	SiO_2	Al_2O_3	Fe_2O_3	MgO	CaO	K_2O	Ti	P_2O_5	SO_3	Mn	Ba	Zr	Zn
BOF	27.8	17.2	0.3	11.5	16.6	0.3	0.2	0.04	0.8	0.09	0.08	0.01	0.006
FA	57.3	34.0	3.7	1.6	1.3	0.9	0.6	0.4	0.1	0.04	0.03	0.02	0.01
IOT	24.9	23.9	32.8	0.6	0.2	1.03	0.4	0.08	0.01	0.08	0.01	0.01	0.008

Table 3 Physical properties of steel fibres

Name	Diameter	Length	Aspect ratio	Tensile strength
Brass-coated steel fibre	0.21 mm	13 mm	61.904	3230.737 MPa

Table 4 Characteristics of 12 M—NaOH solution

Description	Values
NaOH Pellets % in 12 M solution	48 (%)
Water %	52 (%)
Specific gravity, (12 M)	1.32
NaOH: Na_2SiO_3—molarity ratio	2.5

Table 5 Characteristics of Na_2SiO_3 powder

Description	Test Result	Specification
Sodium hydroxide as NaOH % by mass	99.76	99.5 min
Sodium carbonate as Na_2SiO_3% by mass	0.21	0.4. max
Chlorides as NaCl % by mass	0.020	0.10 max
Sulphates as Na_2SO_4% by mass	0.004	01.10 max
Silicate as SiO_2% by mass	0.004	0.02 max
Iron as Fe ppm	6	20.00 max
Copper as Cu ppm	BDL	2.00 max
Manganese as Mn ppm	BDL	1.00 max
Chlorates and Perchlorates as Na_2CO_3 ppm	1	10.00 max
Matter insoluble in water % by mass	0.01	0.05 max

4.1.1 Thermogravimetric Analysis (TGA)

Thermogravimetric analysis (TGA) was performed over the BOF slag, FA, and IOT to determine its thermal stability and weight loss characteristics. The materials are subjected to high-temperature conditions, thereby assessing the amount of weight loss recorded as a function of temperature and providing information on its thermal stability and decomposition patterns. The results of TGA are obtained using a thermogravimetric analyser involving a temperature range from 20 to 1000 °C. The graph includes three curves: DTA (differential thermal analysis), DTG (differential thermogravimetry), and TG (thermogravimetry). By analysing the DTA curve, we can identify the temperature ranges at which significant thermal events occur. The DTG curve helps identify the material's thermal stability and decomposition behaviour. The TG curve represents the change in weight of the material as a function of temperature and thereby helps in understanding the thermal stability, volatile content, and composition of the materials.

Basic Oxygen Furnace (BOF) Slag Figure 4 illustrates the TGA curves for BOF slag, which revealed a weight loss of 2.7%. The DTA curve of BOF slag showed a scattered pattern with distinct changes at different temperature ranges. The initial negative values indicate the release of moisture and volatile components in the slag. The upward trend from 150 to 450 °C suggests an exothermic reaction or crystallization process within this temperature range. The dip in the curve at 730 °C could be attributed to the slag's phase transformation or structural changes. The sudden spike at 900 °C indicates an endothermic reaction or the release of gases during further thermal degradation. Overall, the BOF slag exhibited a complex thermal behaviour with potential reactivity and contributions to the geopolymerization process in EGC.

BOF's DTG curve exhibited sharp spikes with ups and downs, indicating various thermal events occurring within the material. The initial negative values correspond to the release of volatiles and moisture. The significant spike at around 650 °C suggests a rapid exothermic or combustion process. The subsequent dip indicates a decrease in the reaction rate or thermal degradation. The overall thermal behaviour of BOF slag suggests its potential contribution to the geopolymerization process and the development of EGC with improved mechanical properties.

The TG curve of BOF slag demonstrated a gradual weight loss, primarily due to the evaporation of moisture and volatiles at lower temperatures. The controlled weight loss observed throughout the testing indicates the stability of the slag and its suitability for high-temperature applications. The minimal weight loss (0.7%) up to 1000 °C suggests the retention of essential components and reinforces the potential of BOF slag in EGC formulations.

Fly Ash (FA) Figure 5 shows the TGA plot for the proposed fly ash used. The DTA curve of FA showed a scattered pattern with positive and negative values. It can be observed that FA exhibits a linear decrease in heat flow up to 100 °C, reaching approximately − 6 uV. This trend continues until 200 °C, where minor deflections are observed, indicating the release of moisture and volatiles. A notable change occurs at around 180 °C, as the curve rises gradually, reaching a peak at 430 °C (− 2 uV). This suggests an endothermic reaction or the decomposition of carbonates or other compounds in FA. The subsequent decrease in the curve from 430 to
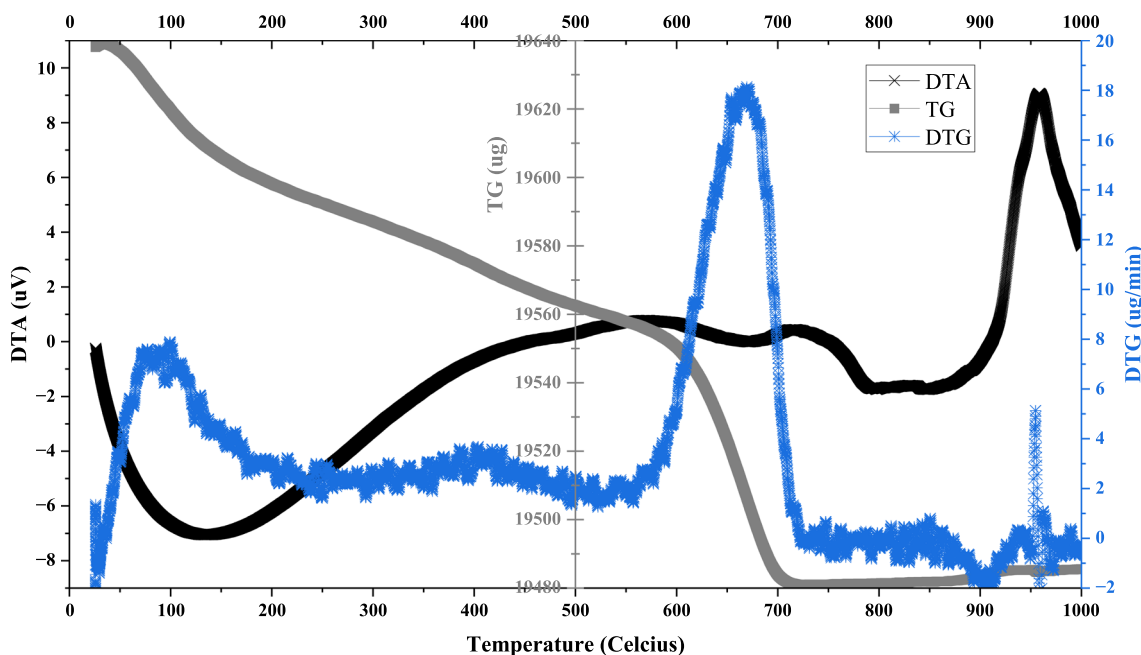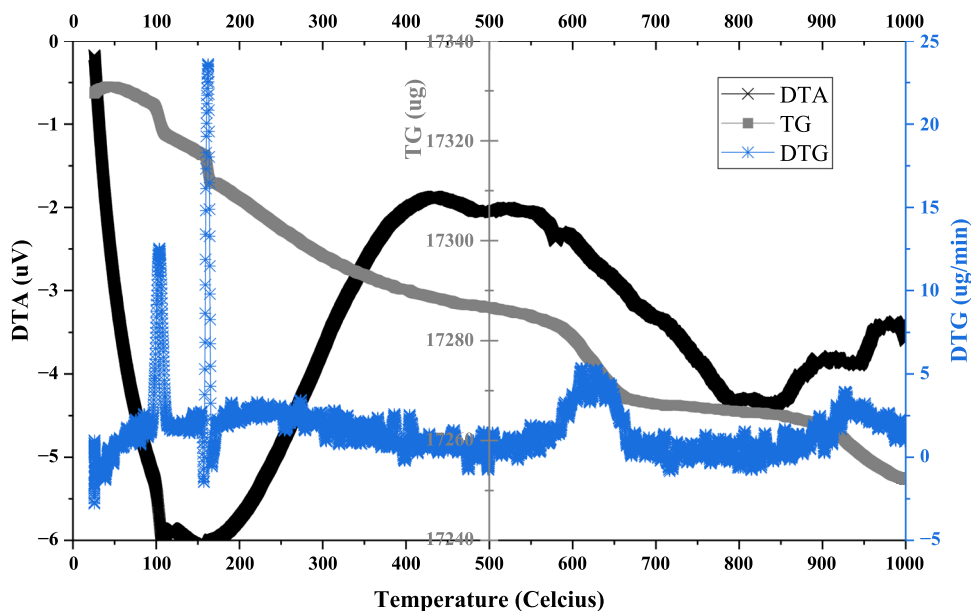
Fig. 4 TGA analysis—BOF slag

Fig. 5 TGA analysis—fly ash

800 °C, with a value of approximately − 4.5 uV at 800 °C, indicates the thermal degradation of organic components and further reactions. The curve remains steady up to 850 °C and exhibits a small spike at 900 °C (− 3.8 uV) and 1000 °C (− 3.2 uV). The overall thermal behaviour of fly ash highlights its potential reactivity and contribution to the geopolymerization process in EGC.

The DTG curve of FA exhibited sharp spikes and fluctuations, indicating various thermal events taking place within the material. Initially, the curve shows a linear upward trend, ranging from − 1 to 2 ug/min, up to 100 °C, corresponding to the release of volatiles and the combustion of organic matter. Sharp spikes and dips in the plot were observed within short temperatures, from 100 to 110 °C (2–12 ug/min) and 150–170 °C (− 1–23 ug/min). The relatively steady behaviour after 170 °C suggests a reduced reactivity or thermal stability of FA fluctuating between 0 and 2.5 ug/min. However, the spike observed between 600 and 650 °C suggests the presence of reactive components within this temperature range. These thermal characteristics
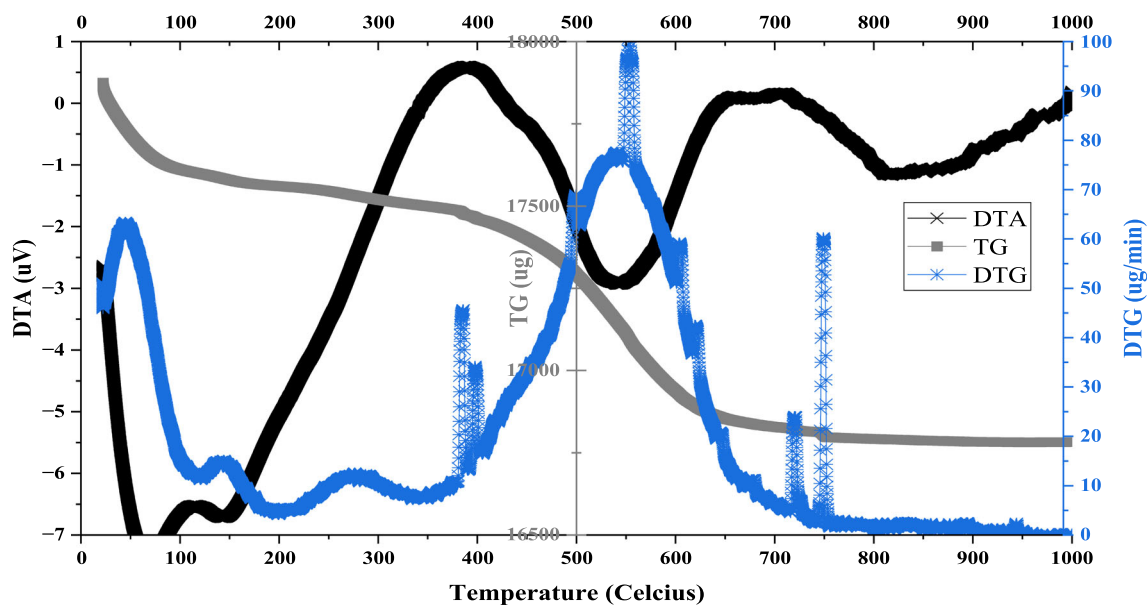
Fig. 6 TGA analysis—IOT

indicate the potential of FA for geopolymerization reactions and its role in improving the properties of EGC.

The TG curve of FA displayed thermal stability up to high temperatures, with minimal weight loss (maintaining a steady value of 17.25 mg up to 1000 °C). The controlled weight loss observed throughout the testing indicates the stability of FA and its suitability for high-temperature applications. The DTA curve shows that FA experiences a significant exothermic reaction around 430 °C, which may be associated with a phase transformation. The DTG curve highlights various volatile components within FA, leading to fluctuating thermal decomposition. The relatively low weight loss (0.46%) up to 1000 °C further emphasizes the retention of essential elements and underscores fly ash as a promising ingredient for the development of EGC.

Iron Ore Tailings (IOT) The TGA plot for the IOT showing the various curves is depicted in Fig. 6. The DTA curve for IOT demonstrates a linear decrease in heat flow up to 70 °C, reaching a minimum of − 7.2 uV. This initial decline is followed by a relatively stable range between − 7.2 uV and − 6.8 uV up to 150 °C. Subsequently, the curve shows a steady increase, reaching a peak value of 1 uV at 400 °C. The curve gradually decreases from 400 to 550 °C, reaching − 3 uV at 550 °C. It remains relatively stable from 550 to 650 °C at 0 uV and maintains this value up to 750 °C. Beyond 750 °C, minimal changes are observed, with the curve slightly increasing to 0.2 uV at 1000 °C.

The DTG curve of IOT displays sharp spikes and fluctuations, similar to a stock chart. Initially, the curve exhibits

a linear upward trend, ranging from 48 to 62 ug/min, up to 50 °C. A sudden dip is observed from 50 to 120 °C, with the DTG value decreasing from 62 to 12 ug/min. From 120 to 380 °C, the DTG values fluctuate between 5 and 15 ug/min with nonlinear variations. Subsequently, a sharp spike is observed at 400 °C, reaching a maximum of 42 ug/min, followed by a sudden drop to 15 ug/min at 420 °C. Beyond 420 °C, the curve experiences a drastic upward trend, reaching a peak value of 110 ug/min at 550 °C. From 550 to 1000 °C, the DTG curve exhibits a linear downward trend, gradually decreasing to 0 ug/min at 1000 °C.

The TG curve reveals weight loss characteristics of IOT during the TGA analysis. The initial weight of the sample (17.88 mg) remains constant, up to 30 °C. Afterwards, a gradual weight reduction is observed, following a nonlinear exponential curve. At 100 °C, the weight reduces to 17.55 mg and decreases to 17.35 mg at 500 °C. Beyond 700 °C, the weight loss stabilizes, maintaining a steady value of 16.8 mg at 1000 °C. The maximum weight loss from the start of the test (0 °C) until the end (1000 °C) is approximately 5.6%.

Based on the above results, it can be inferred that IOT is a suitable material for incorporation into EGC. Its stable structure up to 1000 °C, good thermal stability, and low weight loss make it a promising candidate for the development of EGC. The use of IOT in EGC can also contribute to reducing environmental waste and conserving natural resources.

The thermal stability analysis is performed using thermogravimetric analysis (TGA), revealing the presence of different weight loss stages and providing insights into the materials' thermal behaviour up to 1000° C.

Table 6 Fly ash, IOT and SF percentages used in the study

Constituents	Percentages
FA	100, 90, 80, 70, 60, 50
BOF	0, 10, 20, 30, 40, 50
SF	0.8, 1, 1.5, 1.8, 2
IOT	0, 10, 20, 35, 45

4.2 Mixture Proportions

FA, BOF, IOT and steel fibre (SF) percentages used in this study are shown in Table 6. By varying these parameters, a total of 150 mixes were made. A total of 6 cubes were cast from each mix; for 7 and 28-day strength tests; making a total of 900 cubes for the study. However, the ultimate strength (28 day) was considered crucial and of concern in this study. The 7-day strength was assessed to know the variation of strength between 7 and 28 days (Fig. 14). A 20% extra addition is included in the final volume to consider all the losses that may occur during the casting. The proposed EGC design mix specifications are shown in Table 7. Accordingly, the required amount of raw materials was purchased. The sand-to-binder ratio (s/b) of 0.3 was used in this study. From the studies conducted by Bellum et al. [81], an alkali-to-binder ratio of 0.45 and NaOH/Na$_2$SiO$_3$ molarity ratio of 2.5 were chosen for this experiment.

4.3 Specimen Preparation

The mixing of EGC was initiated upon prior preparation of the alkali activator solution [82]. The solid anhydrous sodium hydroxide pellets were dissolved in the requisite tap water and allowed to cool down for 24 h. All raw materials were weighed and added to the mixer, ensuring uniform mixing of the ingredients. Initially, FA, BOF slag, and anhydrous sodium meta-silicate powder were dry mixed in the Hobart mixer for five minutes and rotated at medium speed. Later, the

cooled down alkali activator solution was added to the mixer, with water having 10% binder volume. It was mixed at a high speed in the mixer for three minutes. Following, the mixer was stopped, and steel fibres were added and rotated at low speeds. When the fibres have fanned out, high speed rotation was done for three minutes for it to get homogenously dispersed throughout the mix. The fibre dispersion and addition methods were according to previous research recommendations [83], and the entire mixing process required around 15 min. The mixes were poured into the greased moulds in two layers and properly tamped to avoid air pockets. The surface of the semi-solid is levelled. The samples were covered with tight plastic sheets to avoid contact with atmospheric moisture. Afterwards, all samples were oven cured for the initial 24 h (Fig. 7a) and followed by ambient curing by wrapping the samples in thick plastic sheets to ensure that no leaching occurred in the EGC samples that might result in unnecessary deterioration of properties for the rest of the period until their ultimate strength attainment (Fig. 7b).

4.4 Compressive Strength

The compressive strength of all the EGC trial mixes prepared was evaluated according to ASTM C109 on 50-mm cube specimens after 7 and 28 days of curing [84]. Three specimens were prepared and tested for each material variable listed in Table 6, thereby allowing the calculation of standard deviations and the mean strength. The experimental tests were performed by applying pressure with a constant loading rate of 1800 N/sec

4.5 Flexural strength

The flexural strength of various mixes was studied using the three-point load method (Fig. 8) according to ASTM C78/C78M-18 [85]. Prismatic specimens of dimensions 50 × 50 × 200 mm were to validate the ultimate load and the corresponding flexural strength upon attaining their 7- and 28-day strength period.

Table 7 Engineered geopolymer composite (EGC) mix specifications

Materials	SF 0.8%	SF 1%	SF 1.5%	SF 1.8%	SF 2%
Binder (kg/m^3)	1562.4	1559.25	1551.375	1546.65	1543.5
Sand (kg/m^3)	520.8	519.75	517.125	515.55	514.5
Fibres (kg/m^3)	16.8	21	31.5	37.8	42
NaOH (kg/m^3)	468.72	467.77	465.412	463.99	463.05
Na$_2$SiO$_3$ (kg/m^3)	234.36	233.88	232.7	231.99	231.525

Fig. 7 **a** Oven curing **b** ambient cured samples

(a)

(b)

Fig. 8 Flexural strength test setup
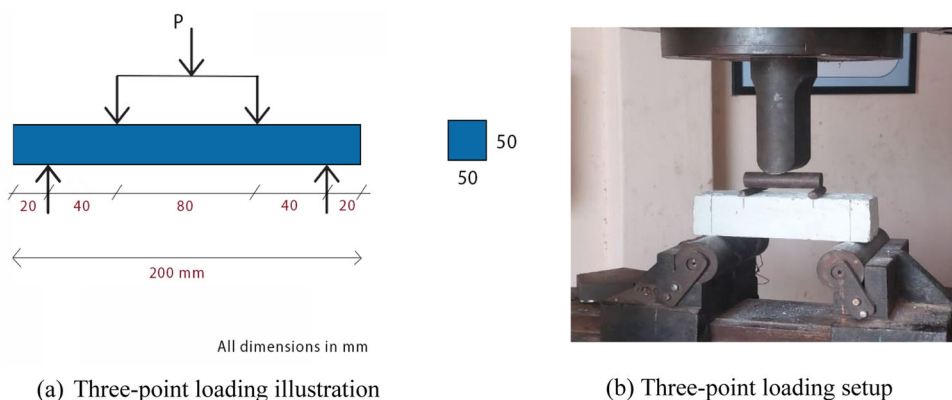
(a) Three-point loading illustration

(b) Three-point loading setup

5 Results and Discussions

5.1 Compressive Strength

The compressive strength (CS) was measured using the compressive strength testing machine (CTM) complying with IS: 516-1959 at the age of 7 and 28 days (CS 7 and CS 28). Three specimens were prepared and tested for each material variable listed (Table 8), thereby allowing the calculation of mean average strength. The experimental tests were performed by applying pressure with a constant loading rate of 1800 N/sec.
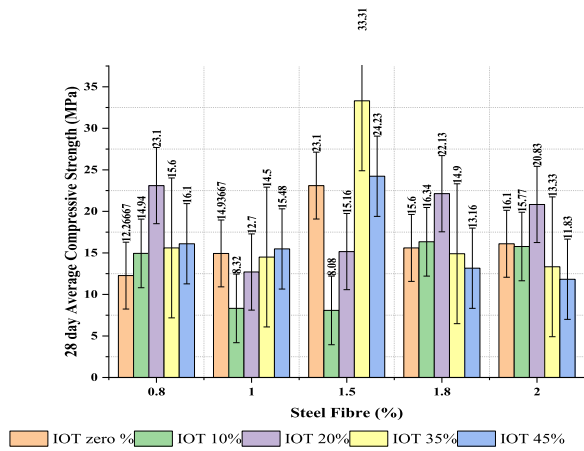
5.1.1 Inferences

From the average 7- and 28-day compressive strengths listed, the ultimate strength attainment at 28 days was considered for the overall 150 mixes. The compressive strength plot (28 days) is shown in Fig. 9. Also, Fig. 10 shows the combined plot showing the compressive strength variation against all three parameters. The highest strength achieved is 41.77 MPa and achieved at 60% FA, 1.5%SF and 45% IOT content, which is evident in the graph. The trend followed by average 28-day compressive strength against the three parameters is shown in Figs. 11, 12, and 13. It can be observed from Fig. 13 that there is a significant linear increase in compressive strength to IOT. At 35% replacement
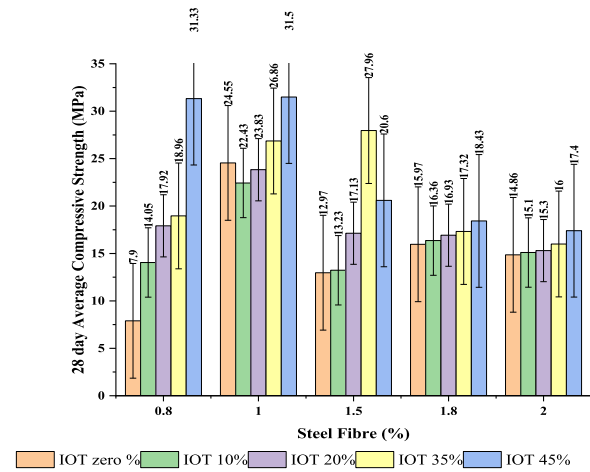
of m-sand with IOT, the average strength increased by 60% when compared to the mixes without IOT. Strength dipped at 45% replacement, possibly due to an increase in shrinkage caused by IOT particles. This can be attributed to the physical characteristics of the IOT particles. IOT typically consists of fine particles with irregular shapes and high surface area. Also, having high water absorption capacity due to their porous and irregular microstructures, upon adding to the EGC matrix, at high replacement levels (45% in this case), the IOT particles absorb a significant amount of water from the mixture causing an increase in the overall water demand of the EGC mix. This reduces the water requirement for the geopolymerization reaction between the FA: BOF and the activated alkaline solutions. The resulting incomplete geopolymerization leads to weaker geopolymer bonds and reduced compressive strength development and shrinkage. Adding BOF slag caused a sudden increase in strength compared to full FA combination, as seen in Fig. 11. This may be attributed to the angular and tough texture of BOF slag and its high alkalinity. This was in line with past studies showing enhanced strength with increased slag content [86–88]. Moreover, this phenomenon can be attributed to several factors. BOF slag having an angular and tough texture enhances the interlocking effect within the EGC matrix. This effect improves the load transfer action and contributes to the overall strength development of the EGC [89]. Additionally, BOF

Table 8 Average 7- and 28-day compressive strengths of the proposed EGC mixes
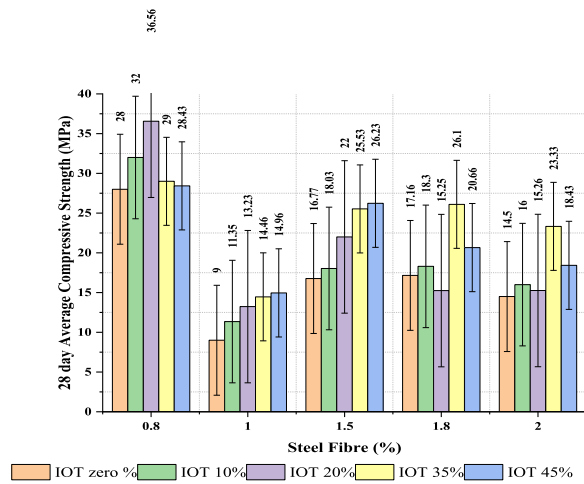
Steel fibre (%)	Fine Aggregate IOT replacement (%)	Average 7-day Compressive strength(MPa)						Average 28-day compressive strength(MPa)					
		100% FA	90% FA	80% FA	70% FA	60% FA	50% FA	100% FA	90% FA	80% FA	70% FA	60% FA	50% FA
0.80	0	9.7	26.2	22.7	5.1	4.9	12.6	12.2	28	24.2	7.9	6.1	13.7
	10	10.5	30.2	23.0	8.6	12.5	19.6	14.9	32	24.6	14	13.2	20.6
	20	21.3	35.2	34.4	12.8	10.4	19.4	23.1	36.5	35	17.9	11.9	20.6
	35	13.4	27.8	33.7	12.7	19.6	23.1	15.6	29	35.4	18.9	24.2	23.7
	45	9.3	26.4	26.8	24.9	11.5	10.8	16.1	28.4	28.8	31.3	13.7	11
1.00	0	6.6	6.6	7.4	16.4	15.4	16.4	12.8	9	8.53	24.5	17.7	19.1
	10	3.8	7.1	9.4	12.4	18.4	23.8	8.3	11.3	12.9	22.4	22	24.5
	20	6.5	8.3	11.5	16.6	22.0	23.6	12.6	13.2	15.4	23.8	22.7	28.3
	35	5.2	9.4	11.6	22.9	23.4	23.6	14.5	14.4	13.7	26.8	34.1	30
	45	6.9	10.5	14.4	29.8	24.9	26.0	15.4	14.9	15.7	31	28	26.9
1.50	0	5.5	12.0	12.5	11.6	8.3	9.4	8.6	16.7	15.2	12.9	19.4	21.3
	10	7.4	15.2	13.9	11.9	12.1	10.7	8.08	18	17.8	13.2	32.5	24.1
	20	12.5	19.9	17.8	15.8	14.4	9.3	15.1	22	18.9	17.1	36.7	30.9
	35	22.8	23.2	35.5	26.1	22.6	14.8	33.3	25.5	35.9	27.9	31.6	28.1
	45	22.0	24.6	29.9	18.9	24.2	16.4	24.2	26.2	34.3	20.6	41.7	32.5
1.80	0	11.8	14.2	12.3	14.0	12.1	13.0	14.2	17.1	14.2	15.9	14.3	15.6
	10	13.1	16.3	16.0	14.3	13.2	12.9	16.3	18.3	17.7	16.3	15.3	15.3
	20	14.0	13.6	20.6	14.5	14.0	14.8	22.13	15.3	21.8	16.9	16.2	17.1
	35	11.2	22.9	26.0	15.4	25.2	22.0	14.9	26.1	27.3	17.3	27.4	24.4
	45	10.2	18.2	20.0	16.3	21.8	18.3	13.1	20.6	22	18.4	23.1	20.6
2.00	0	9.6	12.7	11.0	12.0	10.4	11.0	11.9	14.5	12.6	14.8	11.4	12.6
	10	12.2	14.3	15.0	12.9	11.3	10.8	15.7	16	18.9	15.1	14	12.4
	20	13.6	11.6	18.3	13.2	12.3	13.0	20.8	15.2	21.8	15.3	14.9	16.5
	35	8.8	21.5	22.6	13.4	23.1	19.5	13.3	23.3	24	16	26	21.1
	45	8.6	16.2	18.4	15.4	20.8	16.6	11.8	18.4	20.1	17.4	22	18
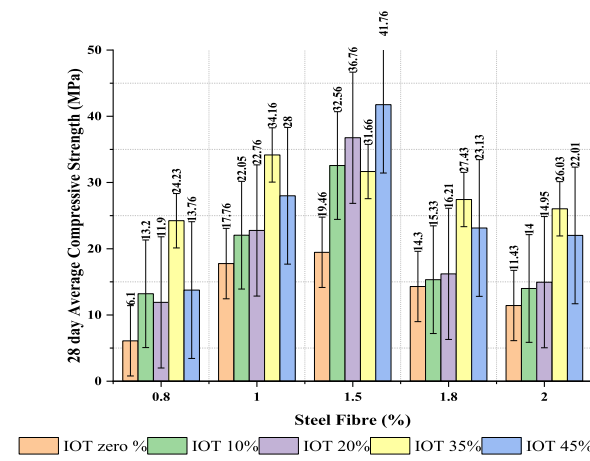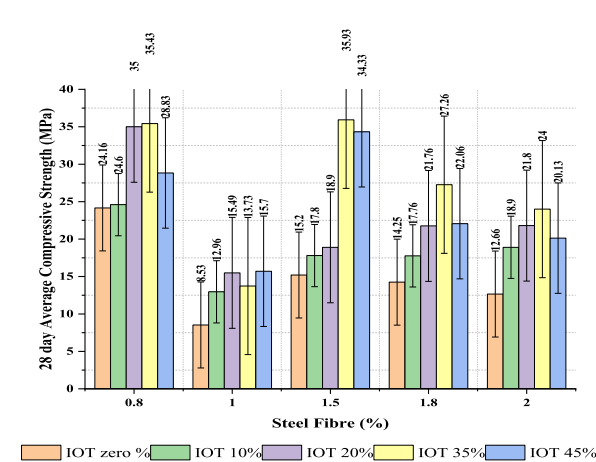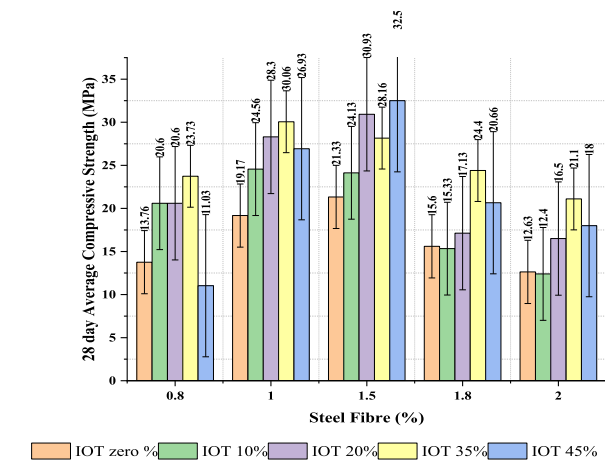
Fig. 9 Average 28-day compressive strength (CS28) for the various (FA: BOF) EGC mixes

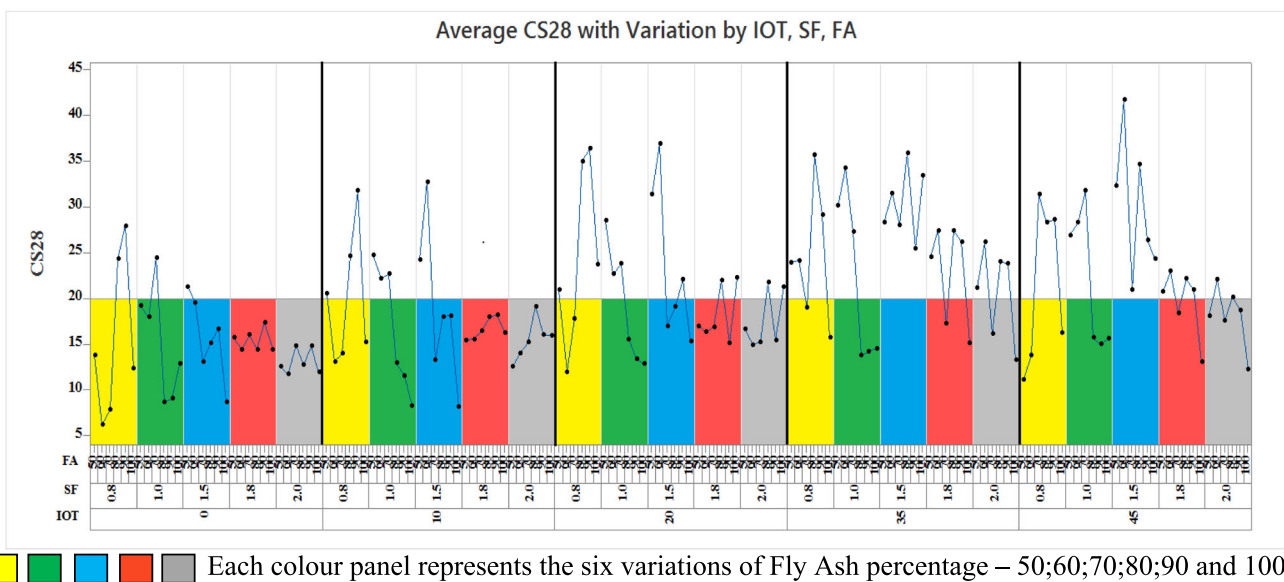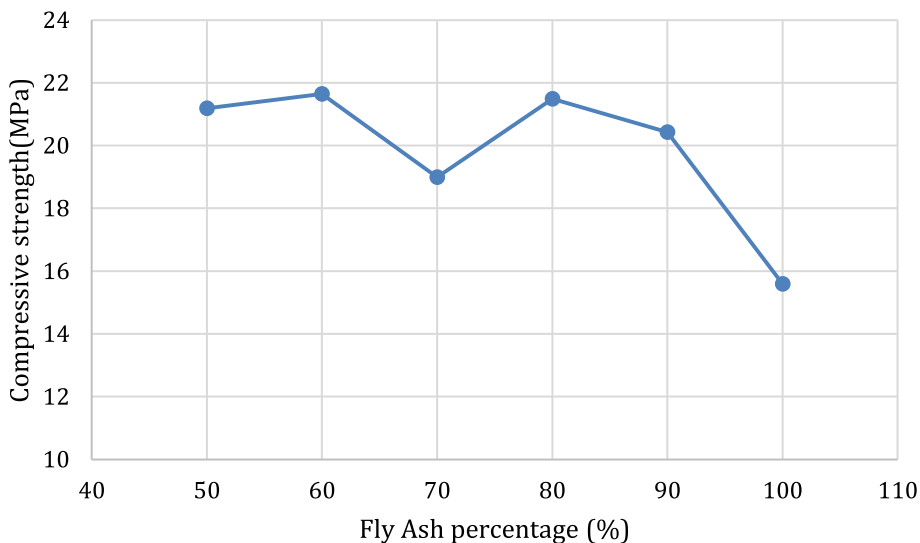Each colour panel represents the six variations of Fly Ash percentage – 50;60;70;80;90 and 100

Fig. 10 Multi-vari chart—average 28-day compressive strength (CS28)
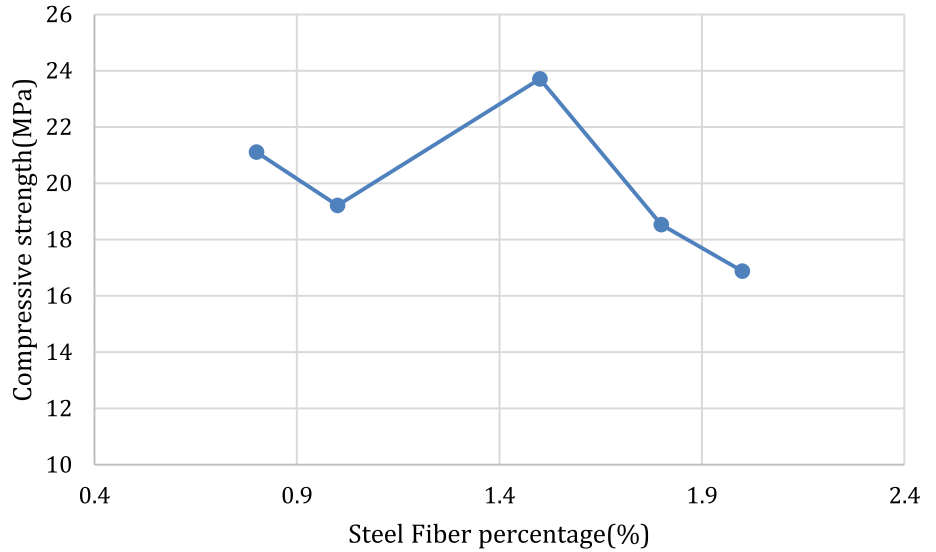
Fig. 11 Effect of replacement of FA by BOF slag on the ultimate compressive strength (CS 28)
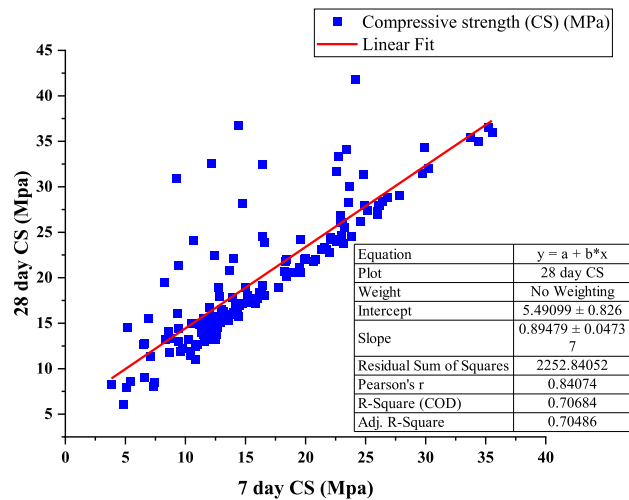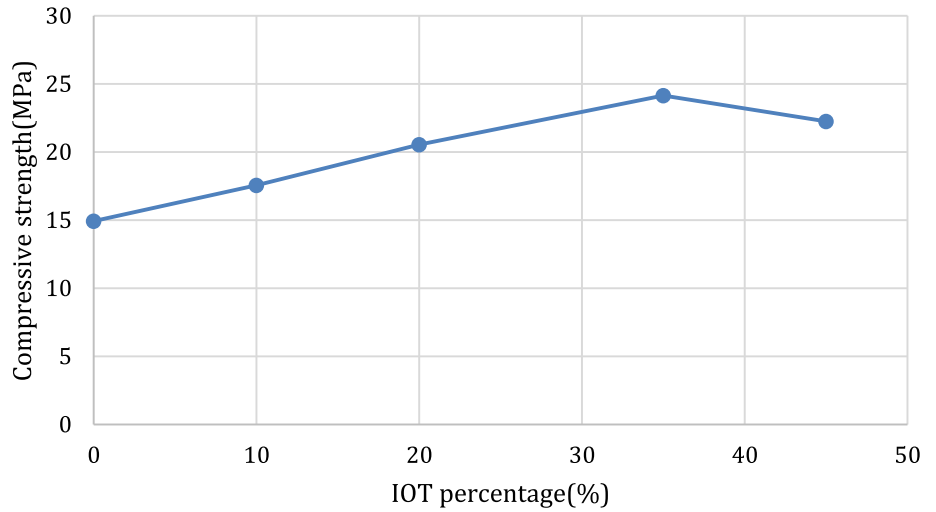

slag possesses high alkalinity considering its chemical composition, with a significant amount of calcium oxide (CaO) [90]. The high alkalinity of BOF promotes the geopolymerization reaction by providing a feasible environment for the activation of FA and aids in the dissolution of silica and alumina from FA particles, thereby forming geopolymeric gels that contribute to the strength development of EGC [91]. 40% FA replacement with BOF slag showed an average strength of 39% greater than 100% fly ash mixes, but the growth observed at 10% replacement started shrinking thereafter. At 1.5% SF combination, the strength peaked, but generally, the increase in the SF composition showed a trend of decrease in strength, as shown in Fig. 12 [92–94]. Figure 14 compares the 7- and 28-day compressive strengths of the EGC specimens. It can be observed that they have comparable values as the

R-square value accounts for (~ 0.706). This result is in accordance with the well-known property of geopolymer concrete to have high early compressive strengths [95–97]. Table 9 details the average ratio of 7 and 28-day strength. The frequency distribution of the strengths shown in Fig. 15 shows that compressive strength of 10.8–15.5 MPa is the most frequent in the test results. Figure 16 shows the box plot of compressive strength values. Here, we can see that 50% of the values lie between the first quartile ($Q1$), at 14.775 MPa, and the third quartile ($Q3$), at 24. 275 MPa. The values have an interquartile range of 9.5 MPa. The highest value observed during testing (41.77 MPa) is an outlier point. The top and bottom whisker points are 36.77 and 6.1 MPa. The median of the values can be observed in the plot as 17.96 MPa.

Fig. 12 Effect of SF on the ultimate compressive strength (CS 28)

Fig. 13 Effect of IOT on the ultimate compressive strength (CS 28)

Equation	y = a + b*x
Plot	28 day CS
Weight	No Weighting
Intercept	5.49099 ± 0.826
Slope	0.89479 ± 0.0473 7
Residual Sum of Squares	2252.84052
Pearson's r	0.84074
R-Square (COD)	0.70684
Adj. R-Square	0.70486

Fig. 14 7-day versus 28-day compressive strength (CS7 vs. CS28)

Despite this, in the case of FA/BOF-based EGC, out of all 150 mix combinations considered, at least one mix per binder combination, regardless of the SF and IOT %, was able to exceed the compressive strength of conventional concrete (M30 ~ 30 MPa) (Fig. 9). As a result, six optimized mixes above this range were obtained (Table 10). This highlights the exceptional strength-to-weight ratio displayed by these materials.

The EGC with the highest compressive strength (EGC-FA: BOF-60:40-MS: IOT-55:45-SF-1.5, attaining (~ 41.8 MPa) can be classified as an effective and sustainable alternative to conventional concrete materials based on IS456:2000 specifications (i.e. 25 MPa > f′c < 55 MPa). Notably, this EGC has a density 13.75% lower than conventional concrete and demonstrates beneficial lightweight properties.

Furthermore, the compressive stress–strain behaviour of all final optimized EGC mixes was determined to know the expected strain-hardening (Fig. 17). Initially, the stress–s-

Table 9 Average ratio of 7- and 28-day compressive strength

Steel fibre (%)	Fine Aggregate IOT replacement (%)	Average ratio of 7 and 28-day compressive strength(MPa)					
		100% FA	90% FA	80% FA	70% FA	60% FA	50% FA
0.80	0	0.80	0.93	0.94	0.64	0.80	0.92
	10	0.71	0.94	0.93	0.62	0.95	0.95
	20	0.92	0.96	0.98	0.72	0.88	0.94
	35	0.86	0.96	0.95	0.67	0.81	0.98
	45	0.58	0.93	0.93	0.79	0.84	0.98
1.00	0	0.52	0.73	0.87	0.67	0.87	0.86
	10	0.46	0.63	0.73	0.55	0.84	0.97
	20	0.52	0.63	0.75	0.70	0.97	0.83
	35	0.36	0.65	0.85	0.86	0.69	0.79
	45	0.45	0.70	0.92	0.96	0.89	0.97
1.50	0	0.63	0.72	0.82	0.90	0.43	0.44
	10	0.91	0.84	0.78	0.90	0.37	0.44
	20	0.83	0.91	0.94	0.92	0.39	0.30
	35	0.68	0.91	0.99	0.94	0.71	0.53
	45	0.91	0.94	0.87	0.92	0.58	0.51
1.80	0	0.83	0.83	0.87	0.88	0.84	0.83
	10	0.81	0.89	0.90	0.88	0.86	0.84
	20	0.63	0.89	0.95	0.86	0.86	0.86
	35	0.75	0.88	0.95	0.89	0.92	0.90
	45	0.78	0.89	0.91	0.89	0.94	0.89
2.00	0	0.81	0.87	0.87	0.81	0.91	0.87
	10	0.78	0.89	0.79	0.86	0.81	0.87
	20	0.66	0.76	0.84	0.86	0.82	0.79
	35	0.66	0.92	0.94	0.84	0.89	0.92
	45	0.73	0.88	0.92	0.88	0.95	0.92

Fig. 15 Frequency distribution of ultimate compressive strength (CS 28)
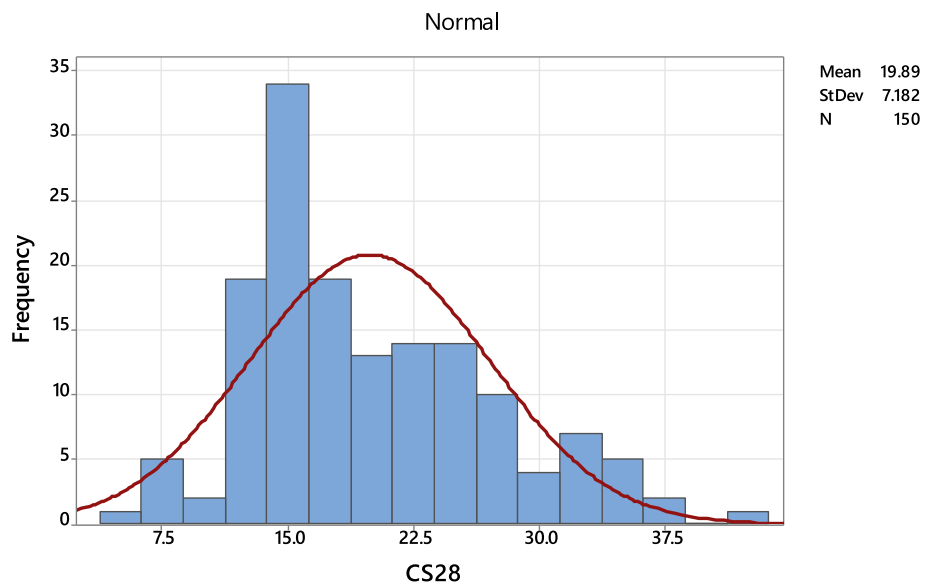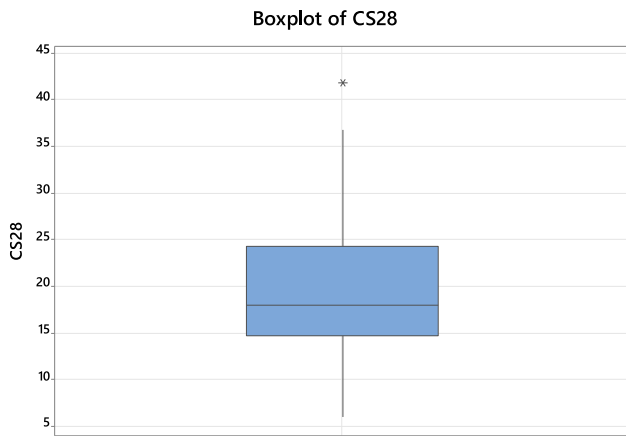
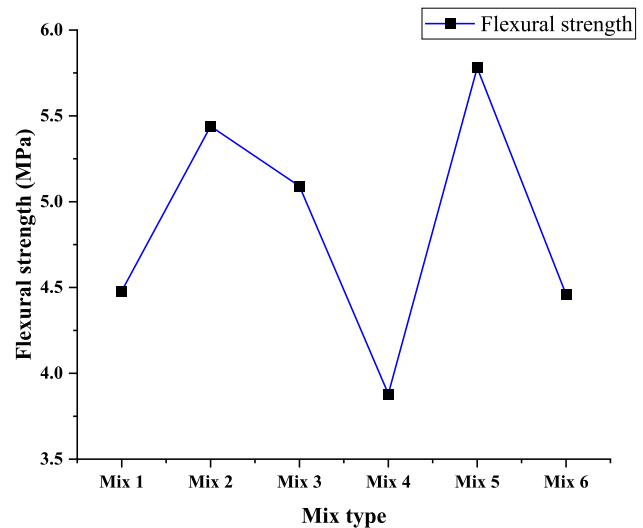**Fig. 16** Boxplot on the ultimate compressive strength (CS 28)

Table 10 Optimized EGC mixes

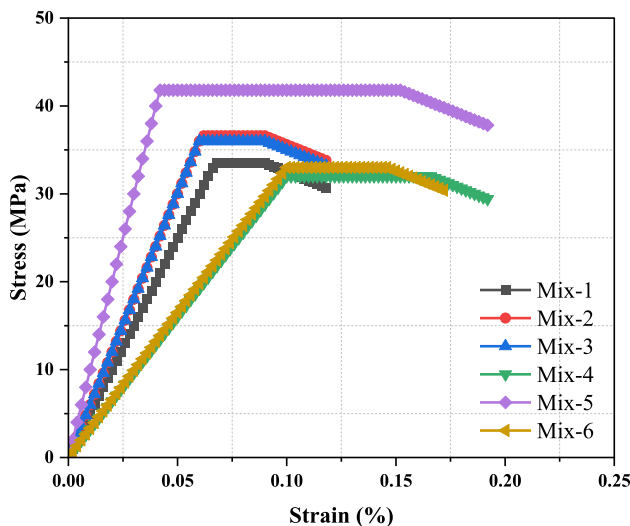| Mix No.	Mix Id
Mix 1	EGC-FA100-MS: IOT-65:35-SF-1.5
Mix 2	EGC-FA: BOF-90:10-MS: IOT-80:20-SF-0.8
Mix 3	EGC-FA: BOF-80:20-MS: IOT-65:35-SF-1.5
Mix 4	EGC-FA: BOF-70:30-MS: IOT-55:45-SF-1
Mix 5	EGC-FA: BOF-60:40-MS: IOT-55:45-SF-1.5
Mix 6	EGC-FA: BOF-50:50-MS: IOT-55:45-SF-1.5

Fig. 17 Typical stress–strain response of optimized EGC mixes
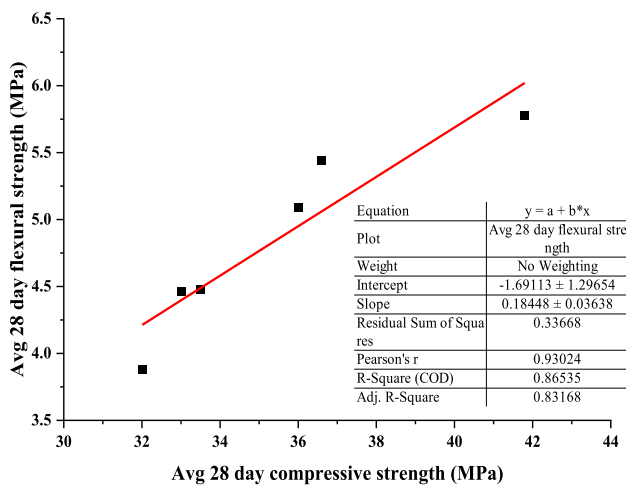
train curve of EGC follows a linear elastic behaviour, similar to other materials. This region is characterized by elastic deformation of the material, with stress released upon the material's return to its original shape. As the strain increases, EGC enters the strain-hardening phase, exhibiting multiple micro-cracking and fibre-bridging mechanisms contributing

Fig. 18 Flexural strength of EGC mixes

to its enhanced ductility. This strain-hardening behaviour allows EGC to sustain higher strains without catastrophic failure. Additionally, EGC reaches its maximum stress or ultimate strength during the strain-hardening phase. This strength is typically higher than that of traditional concrete due to the presence of fibres and optimized mix design. After reaching the ultimate strength, the stress–strain curve gradually decreases, indicating a reduction in load-carrying capacity. However, EGC maintains a significant residual strength even after the peak load, exhibiting good post-peak behaviour.

5.2 Flexural Strength

The flexural strength test results from the sustained flexural load show a complex interaction between the suggested EGC mixtures. Flexural strength ranges from 4.48 to 5.78 M Pa for the proposed mixes (Fig. 18). The measured flexural strengths were mix-1 (4.48 MPa), mix-2 (5.44 MPa), mix-3 (5.09 MPa), mix-4 (3.88 MPa), mix-5 (5.78 MPa), and mix-6 (4.46 MPa). The resistance to bending forces of the EGC mixes followed similar patterns relating to their resistance to compression. Mix-5 (EGC-FA: BOF-60:40-MS: IOT-55:45-SF-1.5) had the highest flexural strength measuring 5.78 MPa. This strength was connected with the highest compressive strength previously determined for the same, thereby improving its resistance to bending forces. Mix-4 (EGC-FA: BOF-70:30-MS: IOT-55:45-SF-1), on the other hand, exhibited the lowest flexural strength (3.88 MPa), indicating a relatively lesser proportion of BOF slag content and SF%, the fact that may have a detrimental effect on their flexural strength. Interestingly, mix-2 (EGC-FA: BOF-90:10-MS: IOT-80:20-SF-0.8) also showed a greater flexural

Equation	y = a + b*x
Plot	Avg 28 day flexural strength
Weight	No Weighting
Intercept	-1.69113 ± 1.29654
Slope	0.18448 ± 0.03638
Residual Sum of Squares	0.33668
Pearson's r	0.93024
R-Square (COD)	0.86535
Adj. R-Square	0.83168

Fig. 19 Correlation between compressive and flexural strength—EGC mixes

strength (5.44 MPa), demonstrating that the higher FA content and MS: IOT may compensate for the lower SF% in terms of flexural strength. Alternatively, mix-3 (EGC-FA: BOF-80:20-MS: IOT-65:35-SF-1.5) exhibited a flexural strength of 5.09 MPa, indicating that increasing the BOF slag content and retaining a modest MS: IOT ratio can still provide high flexural strength, especially at higher SF percentages. Additionally, mix-6 (EGC-FA: BOF-50:50-MS: IOT-55:45-SF-1.5) demonstrated a flexural strength of 4.46 MPa. This implies that a high flexural strength may not always be achieved upon maximum replacement of IOT or slag, especially at higher SF% levels.

5.3 Correlation between Compressive and Flexural Strength

The correlation between flexural strength and compressive strength is proposed as a result of regression analysis of data generated by destructive testing in the laboratory. It is observed that a reasonably good relationship between these two parameters exists for the optimized EGC mixes (Fig. 19).

The regression analysis followed a trendline, represented by the FS = 0.1845 CS − 1.6899 equation, (FS—flexural strength; CS—compressive strength). This equation suggests a positive linear relationship between the compressive strength and flexural strength of the EGC mixes. As the compressive strength increases, the flexural strength increases at a slower rate, as indicated by the slope of (0.18448 ± 0.03638). The R-square value obtained from this linear regression analysis is 0.865, indicating that approximately 86.5% of the variation in flexural strength can be explained by the variation in compressive strength. This high R-square value suggests a strong correlation between the two variables. The adjusted R-square value of 0.83168 further confirms the robustness

of the model, taking into account the number of predictors in the model. The residual sum of squares, a measure of the discrepancy between the data and an estimation model, is relatively low at 0.33668, indicating a good fit of the model to the data. Finally, Pearson's r value of 0.93024 signifies a strong positive correlation between the compressive strength and flexural strength of the EGC mixes. This high correlation coefficient further validates the strong relationship between these two variables, reinforcing the reliability of the regression model.

In conclusion, the correlation study provides a strong and positive relationship between the compressive strength and flexural strength of the optimized EGC mixes. This correlation is crucial in understanding the behaviour of these mixes under different loading conditions, thereby aiding in the design and application of EGC in various structural elements.

5.4 Analysis of Variance (ANOVA)

Analysis of variance (ANOVA) was performed on the test results to find the significance of different parameters and their interactions. The data interpretation was done based on Minitab software. ANOVA is a statistical technique used to compare the means of two or more groups to determine if there are any significant differences. This study used ANOVA to assess the effect of variables (FA/BOF; %IOT and %SF) on compressive strength. ANOVA starts by defining the null and alternative hypotheses. The null hypothesis assumes no differences between group means, while the alternative hypothesis suggests at least one mean is different. ANOVA models vary depending on the study design. The most common ANOVA models are one, two, and repeated measures. The model chosen depends on the number of independent variables and their levels.

Degrees of freedom (DF) indicate the number of independent pieces of info used to estimate population parameters. Degrees of freedom are used to calculate critical values for hypothesis testing. Adj MS is obtained by dividing Adj SS by their degrees of freedom. The mean square between groups (MSB) shows variation between group means, and mean square within groups (MSW) shows variation within each group. The F value is MSB/MSW. The p value measures the probability of getting the observed F-statistic or a more extreme value under the null hypothesis. Compared to a preset significance level (usually 0.05), it helps determine if group mean differences are statistically significant. A p value less than the significance level suggests significant group mean differences, while a higher p value indicates insufficient evidence of difference.

Table 11 Analysis of variance

Source	DF	Adj SS	Adj MS	F Value	P Value
Model	7	1867.36	266.77	6.49	0
Linear	3	1834.54	611.51	14.88	0
FA	1	305.37	305.37	7.43	0.007
SF	1	163.07	163.07	3.97	0.048
IOT	1	1367.35	1367.35	33.27	0
Two-way interactions	3	32.51	10.84	0.26	0.851
FA*SF	1	0.83	0.83	0.02	0.887
FA*IOT	1	31.66	31.66	0.77	0.382
SF*IOT	1	0.03	0.03	0	0.98
Three-way interactions	1	2.58	2.58	0.06	0.803
FA*SF*IOT	1	2.58	2.58	0.06	0.803
Error	142	5836.3	41.1		
Total	149	7703.66			

Fig. 20 Pareto chart of the standardized effects

Pareto Chart of the Standardized Effects
(response is CS28, α = 0.05)
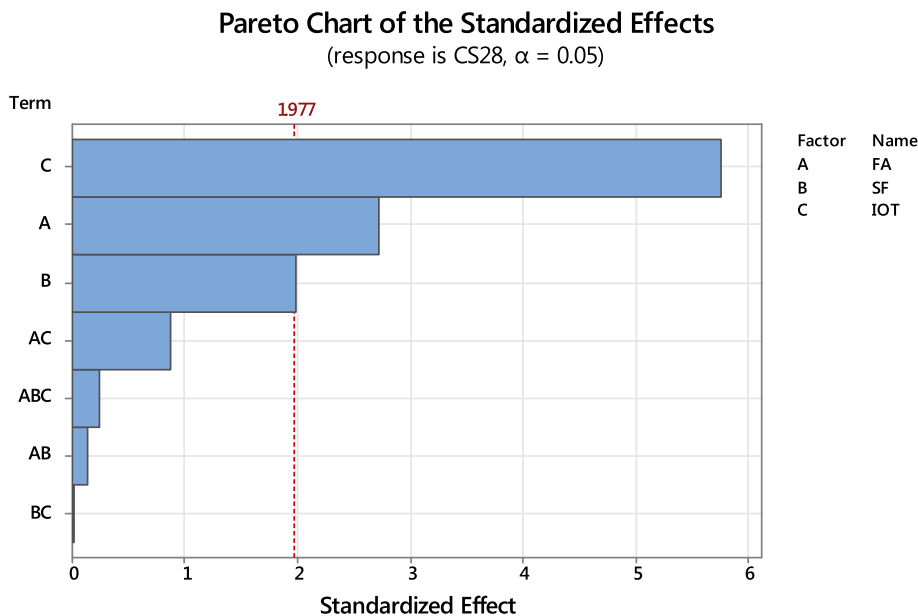
5.4.1 Inferences

Upon analysis and data acquisition by the Minitab software, as shown in Table 11, it was observed that the *p* values of all three independent variables were lower than 0.05, confirming the hypothesis that they significantly affect the compressive strength values. The two and three way interactions were found to be not significant. The same can be seen in the Pareto chart (Fig. 20), where the bars representing factors FA, SF, and IOT cross the reference line at 1.977. These factors are statistically significant at 0.05 with the current model terms. The regression equation found from the analysis is as follows:

$$CS28 = 26.0 - 0.092FA - 4.69SF + 0.204IOT$$
$$+ 0.033FA * SF - 0.00021FA * IOT$$
$$+ 0.075SF * IOT - 0.00103FA * SF * IOT$$

The *R*-squared value and its adjusted and predicted values are 24.24%, 20.51%, and 14.67%, respectively.

While the *R*-squared values being low, it is important to note that the complex nature of the precursors, fine aggregate materials and their parameters involved. EGC being influenced by multiple interactive factors, it is challenging to model with high accuracy using linear regression. However, the regression equation provides useful insights into the rel-

Table 12 Levels of factors

Constituents	Type	Level	Percentages
BOF	Fixed	5	10, 20, 30, 40, 50
SF	Fixed	5	0.8, 1, 1.5, 1.8, 2
IOT	Fixed	5	0, 10, 20, 35, 45

ative impacts of different variables on compressive strength development. Also, the p values from ANOVA confirm that FA, SF, and IOT content each have a statistically significant effect on compressive strength at the 0.05 level. This suggests that the regression equation provides a reasonable fit, capturing the main trends in the data.

5.5 Taguchi Method of Analysis

The Taguchi method of analysis, developed by Genichi Taguchi, is a statistical approach used to optimize product and process designs. It aims to minimize variation and improve quality by identifying and controlling key factors influencing performance. The test methodology consists of two main steps: (1) system design: the design parameters and their respective levels are determined. These parameters are the factors affecting the performance of EGC, and the levels represent the different settings or values each parameter can take. (2) Parameter design: upon fixing the design parameters and levels (FA: BOF; %IOT; %SF), experiments are conducted to determine the optimal combination of parameter settings. Taguchi employs an orthogonal array, a structured experimental design that allows for efficient testing of multiple factors simultaneously with a minimal number of experiments, thereby reducing time and cost. Taguchi emphasizes the "loss function", which quantifies the cost or loss associated with deviations from the desired target value. Considering the loss function, the design can be optimized to minimize the impact of variations and improve overall quality.

5.5.1 Inferences

From Table 12, we infer that there are three parameters (BOF, SF, and IOT) with five levels each. BOF slag replacement is used instead of FA percentage to simplify the calculations. Since the highest value is five, we can use an L25 orthogonal array with three variable parameters, as shown in Table 13.

According to the Taguchi method, the signal-to-noise ratio (S/N) of each machining parameter level must be assessed for each output function to find the optimal machining parameters. The highest S/N of the considered machining parameter levels indicates an optimal level. Minitab software is used for the Taguchi analysis, and the variable parameters along

Table 13 L25 array

Experiment	BOF	SF	IOT
1	10	0.8	0
2	10	1	10
3	10	1.5	20
4	10	1.8	35
5	10	2	45
6	20	0.8	10
7	20	1	20
8	20	1.5	35
9	20	1.8	45
10	20	2	0
11	30	0.8	20
12	30	1	35
13	30	1.5	45
14	30	1.8	0
15	30	2	10
16	40	0.8	35
17	40	1	45
18	40	1.5	0
19	40	1.8	10
20	40	2	20
21	50	0.8	45
22	50	1	0
23	50	1.5	10
24	50	1.8	20
25	50	2	35

Table 14 Response table for S/N ratios

Level	BOF	SF	IOT
1	26.11	26.07	25.3
2	26.33	25.62	24.77
3	25.41	27.53	24.78
4	25.92	25.53	28.44
5	25.06	24.18	25.65
Delta	1.27	3.35	3.67
Rank	3	2	1

with their 28-day compressive strength values, were input to Minitab. Response tables for signal-to-noise ratios are derived as shown in Table 14. Main effect plots for SN ratios are drawn to find the optimum mix conditions shown in Fig. 21.

Since the IOT has the lowest rank (1), it can be inferred that it has the most significant effect on compressive strength; likewise, BOF has the least impact on compressive strength.

Fig. 21 Main effect plot for SN ratios

Main Effects Plot for SN ratios
Data Means

Signal-to-noise: Larger is better
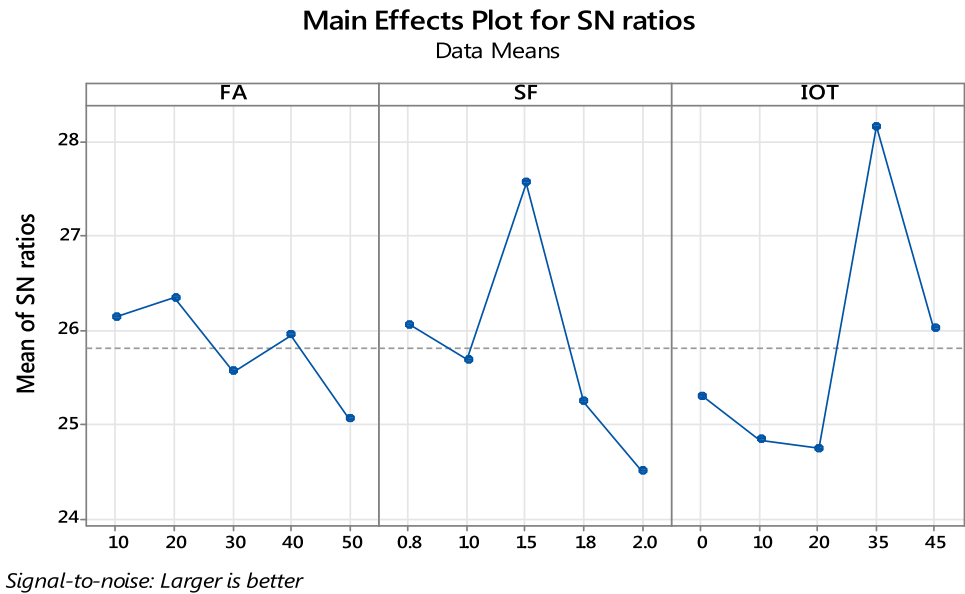
6 Conclusions

A total of 150 mixes or 900 cubes (6 cubes per mix) were prepared to optimize the engineering grade concrete (EGC) with the inclusion of fly ash, basic oxygen furnace slag (BOF slag), iron ore tailings (IOT), and steel fibres (SF). The compressive strengths at 7 days and 28 days were measured and analysed using Taguchi's method and other statistical tools on Minitab software. To gain a better understanding of the trends and influence of the independent variables on the dependent variable, graphs were plotted. For this study, three parameters were varied: the percentage of fly ash (6 levels), the percentage of IOT (5 levels), and the percentage of steel fibre (5 levels). This resulted in a total of 150 mixes. The mixes were classified into six groups based on the fly ash percentage, with each group containing 25 mixes. The mixes with the highest 28-day compressive strengths from each group were selected as the optimum mixes. Thus, each mix represented a unique combination of fly ash. The observations and conclusions are as follows:

- The highest compressive strength achieved was 41.77 MPa, which was obtained with a fly ash percentage of 60%, steel fibre percentage of 1.5%, and IOT percentage of 45%. It was observed that an increase in the percentage of IOT led to a nearly linear increase in strength. The addition of BOF slag as a replacement for fly ash was successful and resulted in a sudden increase in strength, even at a 10% replacement level. The highest strength values were obtained with a steel fibre percentage of 1.5%, although an overall increase in fibre content led to lower compressive strength values.

- All the independent parameters were found to be statistically significant, except for the interactions. According to the Taguchi's method, IOT had the most influence on compressive strength, followed by steel fibre and BOF slag replacement. These findings demonstrate the suitability and potential of BOF slag, fly ash, and IOT in the development of lightweight EGC, which is supported by XRF and TGA analysis.

- The experimental results indicate that the mix consisting of EGC-FA: BOF-60:40-MS: IOT-55:45-SF-1.5 achieved the highest compressive strength (41.8 MPa) and flexural strength (5.78 MPa) among the tested variants. This highlights the potential of steel fibre-reinforced EGC in structural applications. The optimum compressive strength in the EGC was achieved with a steel fibre content of 1.5%, while the most influential parameters on compressive strength were found to be IOT, followed by steel fibre and BOF slag replacement.

Declarations

References

1. Mikulčić, H.; Cabezas, H.; Vujanović, M.; Duić, N.: Environmental assessment of different cement manufacturing processes based on emergy and ecological footprint analysis. J. Clean. Prod. **130**, 213–221 (2016). https://doi.org/10.1016/j.jclepro.2016.01.087

2. Worrell, E.; Price, L.; Martin, N.; Hendriks, C.; Ozawa-Meida, L.: Carbon dioxide emission from the global cement industry. Annu. Rev. Energy Environ. **26**, 303–329 (2001). https://doi.org/10.1146/annurev.energy.26.1.303

3. Chen, C.; Habert, G.; Bouzidi, Y.; Jullien, A.: Environmental impact of cement production: detail of the different processes and cement plant variability evaluation. J. Clean. Prod. **18**, 478–485 (2010). https://doi.org/10.1016/j.jclepro.2009.12.014

4. International Energy Agency (IEA).: Tracking Clean Energy Progress. IEA, Paris (2023). https://www.iea.org/reports/tracking-clean-energy-progress-2023, License: CC BY 4.0

5. International Energy Agency (IEA).: Tracking Industry: Cement (2020). Retrieved from https://www.iea.org/reports/tracking-industry-cement

6. World Steel Association.: World Steel in Figures 2016 (2016). https://www.worldsteel.org/en/dam/jcr:516f8a9e-3b6e-4f0d-8c2c3d8f6a0cbf7c/World%2520Steel%2520in%2520Figures%25202016.pdf

7. Naidu, T.S.; Sheridan, C.M.; van Dyk, L.D.: Basic oxygen furnace slag: review of current and potential uses. Miner. Eng. **149**, 106 (2020)

8. Quader, M.A.; Ahmed, S.; Arif, R.; Ghazilla, R.; Ahmed, S.; Dahari, M.: A comprehensive review on energy efficient CO_2 breakthrough technologies for sustainable green iron and steel manufacturing. Renew. Sustain. Energy Rev. **50**, 594–614 (2015). https://doi.org/10.1016/j.rser.2015.05.026

9. Kuwahara, Y.; Yamashita, H.: A new catalytic opportunity for waste materials: application of waste slag based catalyst in CO_2 fixation reaction. Biochem. Pharmacol. **1**, 50–59 (2013). https://doi.org/10.1016/j.jcou.2013.03.001

10. Helle, M.; Huitu, K.; Helle, H.; Kekkonen, M.; Saxén, H.: Optimization of steelmaking using fastmet DRI in the blast furnace 6th Int. Congress on the Science and Technology of Ironmaking 2012. In: ICSTI 2012 – Including Proceedings from the 42nd Ironmaking and Raw Materials Seminar, and the 13th Brazilian Symp. on Iron Ore 2. pp. 2038–2046

11. Dhunna, R.; Khanna, R.; Mansuri, I.; Sahajwalla, V.: Recycling waste bakelite as an alternative carbon resource for ironmaking applications. ISIJ Int. **54**(3), 613–619 (2014). https://doi.org/10.2355/isijinternational.54.613

12. Hoffmann, C.; Van Hoey, M.; and Zeumer, B.: Decarbonization challenge for steel|McKinsey (2020). www.mckinsey.com. https://www.mckinsey.com/industries/metals-and-mining/our-insights/decarbonization-challenge-for-steel

13. IEA.: Iron and Steel Technology Roadmap. IEA, Paris (2020). https://www.iea.org/reports/iron-and-steel-technology-roadmap, License: CC BY 4.0

14. Liu, J.; Wang, D.: Influence of steel slag-silica fume composite mineral admixture on the properties of concrete. Powder Technol. **320**, 230–238 (2017). https://doi.org/10.1016/j.powtec.2017.07.052

15. Humbert, P.S.: CO_2 activated steel slag-based materials: A Review. J. Clean. Prod. **208**, 448–457 (2019). https://doi.org/10.1016/j.jclepro.2018.10.058

16. Yi, H.; Xu, G.; Cheng, H.; Wang, J.; Wan, Y.; Chen, H.: An overview of utilization of steel slag. Procedia Environ. Sci. **16**, 791–801 (2012). https://doi.org/10.1016/j.proenv.2012.10.108

17. Central Electricity Authority Annual Report 2017–18, pp. 1–248. Ministry of Power, Govt of India (2018)

18. Evarts, H.: Turning Iron and Steel Manufacturing Waste into Valuable Materials (2017). Retrieved May 24, 2019. https://engineering.columbia.edu/news/manufacturing-waste-valuable-materials

19. Gomes, H.I.; Mayes, W.M.; Rogerson, M.; Stewart, D.I.; Burke, I.T.: Alkaline residues and the environment: a review of impacts, management practices and opportunities. J. Cleaner Prod. **112**, 3571–3582 (2016). https://doi.org/10.1016/j.jclepro.2015.09.111

20. Shen, H.; Forssberg, E.: An overview of recovery of metals from slags. Waste Manag. **23**, 933–949 (2003). https://doi.org/10.1016/S0956-053X(02)00164-2

21. Dolage, D.A.R.; Dias, M.G.S.; Ariyawansa, C.T.: Offshore sand as a fine aggregate for concrete production. Br. J. Appl. Sci. Technol. **3**, 813–825 (2013)

22. Devi, B.; Natesh, M.G.; Praveen, K.; Archana, N.; Sogi, A.: An experimental study on utilization of iron ore tailings (IOT) and waste glass powder in concrete. Civ. Environ. Res. **7**, 18 (2015)

23. Pedro, D.D.; Castro, G.B.; Lima, M.M.F.; Lima, R.M.F.: Characterisation and magnetic concentration of an iron ore tailings. J. Mater. Res. Techn. **8**(1), 1052–1059 (2019). https://doi.org/10.1016/j.jmrt.2018.07.015

24. Liu, W.B.; Yao, H.Y.; Wang, J.F.; Chen, C.M.; Liu, Y.T.: Current situation of comprehensive utilization of iron tailings. Mater. Rep. **34**(Z1), 268–270 (2020)

25. Davidovits, J.: Geopolymers: inorganic polymeric new materials. J. Therm. Anal. Calorim. **37**(8), 1633–1656 (1991)

26. Duxson, P.; Provis, J.L.: Designing precursors for geopolymer cements. J. Am. Ceram. Soc. **91**(12), 3864–3869 (2008)

27. Kumar, S.; Chen, B.; Xu, Y.; Dai, J.-G.: Structural behavior of FRP grid reinforced geopolymer concrete sandwich wall panels subjected to concentric axial loading. Compos. Struct. **270**, 114117 (2021). https://doi.org/10.1016/j.compstruct.2021.114117

28. Huang, J.-Q.; Dai, J.-G.: Flexural performance of precast geopolymer concrete sandwich panel enabled by FRP connector. Compos. Struct. **248**, 112563 (2020). https://doi.org/10.1016/j.compstruct.2020.112563

29. Li, V.C.; Leung, C.K.Y.: Steady-state and multiple cracking of short random fiber composites. J. Eng. Mech. **118**(11), 2246–2264 (1992)

30. Li, V.C.; Mishra, D.K.; Wu, H.-C.: Matrix design for pseudo-strain-hardening fibre reinforced cementitious composites. Mater. Struct. **28**(10), 586–595 (1995)

31. Li, V.C.; Wang, S.; Wu, C.: Tensile strain-hardening behavior of polyvinyl alcohol engineered cementitious composite (PVA-ECC). ACI Mater. J. Am. Concr. Inst. **98**, 483–492 (2001)

32. Kanda, T.; Li, V.C.: Practical design criteria for saturated pseudo strain hardening behavior in ECC. J. Adv. Concr. Technol. **4**(1), 59–72 (2006)

33. Li, V.C.; Horii, H.; Kabele, P.; Kanda, T.; Lim, Y.M.: Repair and retrofit with engineered cementitious composites. Eng. Fract. Mech. **65**(2–3), 317–334 (2000)

34. Chen, Y.; Yu, J.; Leung, C.K.Y.: Use of high strength strain-hardening cementitious composites for flexural repair of concrete structures with significant steel corrosion. Constr. Build. Mater. **167**, 325–337 (2018)

35. Yang, X.; Gao, W.-Y.; Dai, J.-G.; Lu, Z.-D.; Yu, K.-Q.: Flexural strengthening of RC beams with CFRP grid-reinforced ECC matrix. Compos. Struct. **189**, 9–26 (2018)

36. Yang, X.; Gao, W.-Y.; Dai, J.-G.; Lu, Z.-D.: Shear strengthening of RC beams with FRP grid-reinforced ECC matrix. Compos. Struct. **241**, 112120 (2020). https://doi.org/10.1016/j.compstruct.2020.112120

37. Gao, W.-Y.; Hu, K.-X.; Dai, J.-G.; Dong, K.; Yu, K.-Q.; Fang, L.-J.: Repair of fire- damaged RC slabs with basalt fabric-reinforced shotcrete. Constr. Build. Mater. **185**, 79–92 (2018)

38. Ohno, M.; Li, V.C.: A feasibility study of strain hardening fiber reinforced fly ash-based geopolymer composites. Constr. Build.

Mater. **57**, 163–168 (2014). https://doi.org/10.1016/j.conbuildmat.2014.02.005

39. Lee, B.Y.; Cho, C.-G.; Lim, H.-J.; Song, J.-K.; Yang, K.-H.; Li, V.C.: Strain hardening fiber reinforced alkali-activated mortar—a feasibility study. Constr. Build. Mater. **37**, 15–20 (2012)

40. Nematollahi, B.; Sanjayan, J.; Qiu, J.; Yang, E.-H.: High ductile behavior of a polyethylene fiber-reinforced one-part geopolymer composite: a micromechanics-based investigation. Arch. Civ. Mech. Eng. **17**(3), 555–563 (2017)

41. Alrefaei, Y.; Dai, J.-G.: Deflection hardening behavior and elastic modulus of one- part hybrid fiber-reinforced geopolymer composites. J. Asian Concr. Fed. **5**(2), 37–51 (2019)

42. Alrefaei, Y.; Dai, J.-G.: Tensile behavior and microstructure of hybrid fiber ambient cured one-part engineered geopolymer composites. Constr. Build. Mater. **184**, 419–431 (2018)

43. Lao, J.C.; Huang, B.T.; Xu, L.Y.; Dai, J.G.; Shah, S.P.: Engineered geopolymer composites (EGC) with ultra-high strength and ductility. In: Kunieda, M.; Kanakubo, T.; Kanda, T.; Kobayashi, K. (Eds.) Strain Hardening Cementitious Composites. SHCC 2022. RILEM Bookseries, Vol. 39. Springer, Cham (2023). https://doi.org/10.1007/978-3-031-15805-6_4

44. Elmesalami, N.; Celik, K.: A critical review of engineered geopolymer composite: a low-carbon ultra-high-performance concrete. Constr. Build. Mater. **346**, 128491 (2022). https://doi.org/10.1016/j.conbuildmat.2022.128491

45. Lao, J.-C.; Xu, L.-Y.; Huang, B.-T.; Zhu, J.-X.; Khan, M.; Dai, J.-G.: Utilization of sodium carbonate activator in strain-hardening ultra-high-performance geopolymer concrete (SH-UHPGC). Front. Mater. (2023). https://doi.org/10.3389/fmats.2023.1142237

46. Asrani, N.P.; Murali, G.; Parthiban, K.; Surya, K.; Prakash, A.; Rathika, K.; Chandru, U.: A feasibility of enhancing the impact resistance of hybrid fibrous geopolymer composites: experiments and modelling. Constr. Build. Mater. **203**, 56–68 (2019)

47. Huang, X.; Ranade, R.; Zhang, Q.; Ni, W.; Li, V.C.: Mechanical and thermal properties of green lightweight engineered cementitious composites. Constr. Build. Mater. **48**, 954–960 (2013)

48. Korniejenko, K.; Lin, W.-T.; Šimonová, H.: Mechanical properties of short polymer fiber-reinforced geopolymer composites. J. Compos. Sci. **4**(3), 128 (2020). https://doi.org/10.3390/jcs4030128

49. Guo, L.; Wu, Y.; Xu, F.; Song, X.; Ye, J.; Duan, P.; Zhang, Z.: Sulfate resistance of hybrid fiber reinforced metakaolin geopolymer composites. Compos. B Eng. **183**, 107689 (2020). https://doi.org/10.1016/j.compositesb:2019.107689

50. Sun, R.; Hu, X.; Ling, Y.; Zuo, Z.; Zhuang, P.; Wang, F.: Chloride diffusion behavior of engineered cementitious composite under dry-wet cycles. Constr. Build. Mater. **260**, 119943 (2020). https://doi.org/10.1016/j.conbuildmat.2020.119943

51. Hasan, M.J.; Hossain, K.M.A.: Assessing suitability of geopolymer composites under chloride exposure. In: Walbridge, S., et al. (eds.) Proceedings of the Canadian Society of Civil Engineering Annual Conference 2021. CSCE 2021. Lecture Notes in Civil Engineering, vol. 240. Springer, Singapore (2023). https://doi.org/10.1007/978-981-19-0507-0_35

52. Nematollahi, B.; Sanjayan, J.; Shaikh, F.U.A.: Matrix design of strain hardening fiber reinforced engineered geopolymer composite. Compos. B Eng. **89**, 253–265 (2016). https://doi.org/10.1016/j.compositesb.2015.11.039

53. Yip, C.K.; Lukey, G.C.; Provis, J.L.; van Deventer, J.S.J.: Effect of calcium silicate sources on geopolymerisation. Cem. Concr. Res. **38**(4), 554–564 (2008)

54. Reddy, M.S.; Dinakar, P.; Rao, B.H.: A review of the influence of source material's oxide composition on the compressive strength of geopolymer concrete. Microporous Mesoporous Mater. **234**, 12–23 (2016)

55. Ohno, M.; Li, V.C.: An integrated design method of engineered geopolymer composite. Cem. Concr. Compos. **88**, 73–85 (2018). https://doi.org/10.1016/j.cemconcomp.2018.02.001

56. Shaikh, F.U.A.: Deflection hardening behaviour of short fibre reinforced fly ash based geopolymer composites. Mater. Des. **50**, 674–682 (2013)

57. Al-Majidi, M.H.; Lampropoulos, A.; Cundy, A.B.: Tensile properties of a novel fibre reinforced geopolymer composite with enhanced strain hardening characteristics. Compos. Struct. **168**, 402–427 (2017)

58. Farooq, M.; Bhutta, A.; Banthia, N.: Tensile performance of eco-friendly ductile geopolymer composites (EDGC) incorporating different micro-fibers. Cem. Concr. Compos. **103**, 183–192 (2019)

59. Al-Majidi, M.H.; Lampropoulos, A.; Cundy, A.B.: Steel fibre reinforced geopolymer concrete (SFRGC) with improved microstructure and enhanced fibre-matrix interfacial properties. Constr. Build. Mater. **139**, 286–307 (2017)

60. Wang, Y.; Wang, Y.; Zhang, M.: Effect of sand content on engineering properties of fly ash-slag based strain hardening geopolymer composites. J. Build. Eng. **34**, 101951 (2021). https://doi.org/10.1016/j.jobe.2020.101951

61. Wang, B.; Feng, H.; Huang, H.; Guo, A.; Zheng, Y.; Wang, Y.: Bonding properties between fly ash/slag-based engineering geopolymer composites and concrete. Materials **16**(12), 4232 (2023). https://doi.org/10.3390/ma16124232

62. Zhou, X.; Chen, X.; Peng, Z., et al.: Cleaner geopolymer prepared by co-activation of gasification coal fly ash and steel slag: durability properties and economic assessment. Front. Environ. Sci. Eng. **17**, 150 (2023). https://doi.org/10.1007/s11783-023-1750-9

63. Zhang, Z.; Provis, J.; Reid, A.; Wang, H.: Fly ash-based geopolymers: the relationship between composition, pore structure and efflorescence. Cem. Concr. Res. **64**, 30–41 (2014). https://doi.org/10.1016/j.cemconres.2014.06.004

64. George, G.: Replacement of fine aggregate by iron ore tailing (IOT) in concrete for sustainable development. E3S Web Conf. **387**, 04012 (2023). https://doi.org/10.1051/e3sconf/202338704012

65. Noorvand, H.; Arce, G.; Hassan, M.; Rupnow, T.: Investigation of the mechanical properties of engineered cementitious composites with low fiber content and with crumb rubber and high fly ash content. Transp. Res. Rec. **2673**(5), 418–428 (2019). https://doi.org/10.1177/0361198119837510

66. Kan, L.; Wei Lv, J.; Bei Duan, B.; Wu, M.: Self-healing of engineered geopolymer composites prepared by fly ash and metakaolin. Cem. Concr. Res. **125**(9), 105895 (2019). https://doi.org/10.1016/j.cemconres.2019.105895

67. Osman, B.H.; Sun, X.; Tian, Z.; Lu, H.; Jiang, G.: Dynamic compressive and tensile characteristics of a new type of ultra-high-molecular weight polyethylene (UHMWPE) and polyvinyl alcohol (PVA) fibers reinforced concrete. Shock. Vib. (2019). https://doi.org/10.1155/2019/6382934

68. Choi, J.I.; Lee, B.Y.; Ranade, R.; Li, V.C.; Lee, Y.: Ultra-high-ductile behavior of a polyethylene fiber-reinforced alkali-activated slag-based composite. Cem. Concr. Compos. **70**, 153–158 (2016). https://doi.org/10.1016/j.cemconcomp.2016.04.002

69. Yu, K.Q.; Yu, J.T.; Dai, J.G.; Lu, Z.D.; Shah, S.P.: Development of ultra-high performance engineered cementitious composites using polyethylene (PE) fibers. Constr. Build. Mater. **158**, 217–227 (2018). https://doi.org/10.1016/j.conbuildmat.2017.10.040

70. Ding, Y.; Yu, K.Q.; Tao Yu, J.; Lang Xu, S.: Structural behaviors of ultra-high performance engineered cementitious composites (UHP-ECC) beams subjected to bending-experimental study. Constr. Build. Mater. **177**, 102–115 (2018). https://doi.org/10.1016/j.conbuildmat.2018.05.122

71. Nematollahi, B.; Sanjayan, J.; Shaikh, F.U.A.: Strain hardening behavior of engineered geopolymer composites: effects of the activator combination. J. Aust. Ceram. Soc. **51**(1), 54–60 (2015)

72. Nematollahi, B.; Sanjayan, J.; Shaikh, F.U.A.: Comparative deflection hardening behavior of short fiber reinforced geopolymer composites. Constr. Build. Mater. **70**, 54–64 (2014). https://doi.org/10.1016/j.conbuildmat.2014.07.085

73. Ma, C.; Long, G.; Shi, Y.; Xie, Y.: Preparation of cleaner one-part geopolymer by investigating different types of commercial sodium metasilicate in China. J. Clean. Prod. **201**, 636–647 (2018). https://doi.org/10.1016/j.jclepro.2018.08.060

74. Nematollahi, B.; Sanjayan, J.; Ahmed Shaikh, F.U.: Tensile strain hardening behavior of PVA fiber-reinforced engineered geopolymer composite. J. Mater. Civ. Eng. **27**(10), 1–12 (2015). https://doi.org/10.1061/(ASCE)MT.1943-5533.0001242

75. Alex, T.C.; Mucsi, G.; Venugopalan, T., et al.: BOF steel slag: critical assessment and integrated approach for utilization. J. Sustain. Metall. **7**, 1407–1424 (2021). https://doi.org/10.1007/s40831-021-00435-2

76. Yüksel, İ: A review of steel slag usage in construction industry for sustainable development. Environ. Dev. Sustain. **19**, 369–384 (2017). https://doi.org/10.1007/s10668-016-9759-x

77. Nagajothi, S.; Elavenil, S.: Strength assessment of geopolymer concrete using M-sand. Int. J. Chem. Sci. **14**(S1), 15–21 (2016)

78. Shoaei, P.; Musaeei, H.R.; Mirlohi, F.; Narimani zamanabadi, S.; Ameri, F.; Bahrami, N.: Waste ceramic powder-based geopolymer mortars: effect of curing temperature and alkaline solution-to-binder ratio. Construct. Build. Mater. (2019). https://doi.org/10.1016/j.conbuildmat.2019.116686

79. Nematollahi, B.; Sanjayan, J.: Effect of different superplasticizers and activator combinations on workability and strength of fly ash based geopolymer. Mater. Des. (2014). https://doi.org/10.1016/j.matdes.2014.01.064

80. Hanjitsuwan, S.; Hunpratub, S.; Thongbai, P.; Maensiri, S.; Sata, V.; Chindaprasirt, P.: Effects of NaOH concentrations on physical and electrical properties of high calcium fly ash geopolymer paste. Cem. Concr. Compos. (2014). https://doi.org/10.1016/j.cemconcomp.2013.09.012

81. Bellum, R.R.; Nerella, R.; Madduru, S.R.C.; Indukuri, C.S.R.: Mix design and mechanical properties of fly ash and GGBFS-synthesized alkali-activated concrete (AAC). Infrastructures **4**(2), 20 (2019). https://doi.org/10.3390/infrastructures4020020

82. Alrefaei, Y.; Wang, Y.-S.; Dai, J.-G.: Effect of mixing method on the performance of alkali-activated fly ash/slag pastes along with polycarboxylate admixture. Cem. Concr. Compos. **117**, 103917 (2021). https://doi.org/10.1016/j.cemconcomp.2020.103917

83. Alrefaei, Y.; Rahal, K.; Maalej, M.: Shear strength of beams made using hybrid fiber–engineered cementitious composites. J. Struct. Eng. **144**(1), 04017177 (2018). https://doi.org/10.1061/(ASCE)ST.1943-541X.0001924

84. ASTM C109: Standard test method for compressive strength of hydraulic cement mortars (using 2 – in. or [50 - mm] cube specimens). Chem. Anal. (2010). https://doi.org/10.1520/C0109

85. ASTM International: Standard Test Method for Flexural Strength of Concrete (Using Simple Beam with Third-Point Loading). ASTM C78/C78M-18, ASTM International, West Conshohocken (2018)

86. Humad, A.M.; Kothari, A.; Provis, J.L.; Cwirzen, A.: The effect of blast furnace slag/fly ash ratio on setting, strength, and shrinkage of alkali-activated pastes and concretes. Front. Mater. **6**, 9 (2019). https://doi.org/10.3389/fmats.2019.00009

87. Qiu, J.; Zhao, Y.; Xing, J.; Sun, X.: Fly ash/blast furnace slag-based geopolymer as a potential binder for mine backfilling: effect of binder type and activator concentration. Adv. Mater. Sci. Eng. **2019**, 1–12 (2019)

88. Abhishek, H.S.; Prashant, S.; Kamath, M.V.; Kumar, M.: Fresh mechanical and durability properties of alkali-activated fly ash-slag concrete: a review. Innov. Infrastruct. Solut. (2021). https://doi.org/10.1007/s41062-021-00711-w

89. Lee, W.-H.; Cheng, T.-W.; Lin, K.-Y.; Lin, K.-L.; Wu, C.-C.; Tsai, C.-T.: Geopolymer technologies for stabilization of basic oxygen furnace slags and sustainable application as construction materials. Sustainability **12**(12), 5002 (2020). https://doi.org/10.3390/su12125002

90. Pacheco-Torgal, F.; Castro-Gomes, J.; Jalali, S.: Alkali-activated binders: a Review. Part 2. About materials and binders manufacture. Constr. Build. Mater. (2007). https://doi.org/10.1016/j.conbuildmat.2007.03.019

91. Rovnaník, P.: Effect of curing temperature on the development of hard structure of metakaolin-based geopolymer. Constr. Build. Mater. **24**(7), 1176–1183 (2010). https://doi.org/10.1016/j.conbuildmat.2009.12.023

92. Bahraq, A.A.; Maslehuddin, M.; Al-Dulaijan, S.U.: Macro- and micro-properties of engineered cementitious composites (ECCs) incorporating industrial waste materials: a review. Arab. J. Sci. Eng. **45**, 7869–7895 (2020). https://doi.org/10.1007/s13369-020-04729-7

93. Ye, Y.; Liu, J.; Zhang, Z.; Wang, Z.; Peng, Q.: Experimental study of high-strength steel fiber lightweight aggregate concrete on mechanical properties and toughness index. Adv. Mater. Sci. Eng. **2020**, 10 (2020). https://doi.org/10.1155/2020/5915034

94. Natarajan, K.S.; Yacinth, S.I.B.; Veerasamy, K.: Strength and durability characteristics of steel fiber-reinforced geopolymer concrete with addition of waste materials. Environ. Sci. Pollut. Res. (2022). https://doi.org/10.1007/s11356-022-22360-x

95. Zheng, C.; Wang, J.; Liu, H.; GangaRao, H.; Liang, R.: Characteristics and microstructures of the GFRP waste powder/GGBS-based geopolymer paste and concrete. Rev. Adv. Mater. Sci. **61**(1), 117–137 (2022). https://doi.org/10.1515/rams-2022-0005

96. Nematollahi, B.; Xia, M.; Sanjayan, J.: Enhancing strength of powder-based 3D printed geopolymers for digital construction applications. In: Mechtcherine, V.; Khayat, K.; Secrieru, E. (Eds.) Rheology and Processing of Construction Materials. RheoCon SCC 2019 2019. RILEM Bookseries, Vol. 23. Springer, Cham (2020). https://doi.org/10.1007/978-3-030-22566-7_48

97. Zhang, H.; Li, L.; Sarker, P.K., et al.: Investigating various factors affecting the long-term compressive strength of heat-cured fly ash geopolymer concrete and the use of orthogonal experimental design method. Int. J. Concr. Struct. Mater. **13**, 63 (2019). https://doi.org/10.1186/s40069-019-0375-7

98. Singh, N.B.: Fly ash-based geopolymer binder: a future construction material. Minerals (2018). https://doi.org/10.3390/min8070299